



Available online at [www.sciencedirect.com](http://www.sciencedirect.com)

**SciVerse ScienceDirect**

ELSEVIER

*Acta Materialia* 60 (2012) 2449–2470



[www.elsevier.com/locate/actamat](http://www.elsevier.com/locate/actamat)

Overview No. 151

## Multiferroic and magnetoelectric heterostructures

L.W. Martin <sup>a,\*</sup>, R. Ramesh <sup>b</sup>

<sup>a</sup> Department of Materials Science and Engineering and F. Seitz Materials Research Laboratory, University of Illinois, Urbana-Champaign, Urbana, IL 61801, USA

<sup>b</sup> Department of Materials Science and Engineering and Department of Physics, Lawrence Berkeley National Laboratory, University of California, Berkeley, CA 94720, USA

Available online 25 January 2012

### Abstract

We review recent developments and advances in multiferroic and magnetoelectric heterostructures. Driven by the promise of new materials functionality (i.e. electric field control of ferromagnetism), extensive on-going research is focused on the search for and characterization of new multiferroic materials. In this review we develop a comprehensive overview of multiferroic materials, including details on the nature of order parameters and coupling in these materials, the scarcity of such materials in single phase form, routes to create and control the properties of these materials, and we finish by investigating such effects in a number of model materials and heterostructures. This includes an in-depth discussion of BiFeO<sub>3</sub>, an investigation of recent advances in magnetoelectric materials, and an introduction to a variety of approaches by which one can achieve novel materials functionality.

© 2011 Acta Materialia Inc. Published by Elsevier Ltd. All rights reserved.

**Keywords:** Multiferroics; Magnetoelectrics; BiFeO<sub>3</sub>; Oxide thin films

### 1. Introduction

Complex oxides represent a broad class of materials that have a wide range of crystal structures and functionalities. Among them, the study of magnetic, ferroelectric, and more recently, multiferroic properties has stimulated considerable interest. The study of multiferroic and magnetoelectric materials, in particular, has experienced a dramatic increase in research effort over the past decade and today we see the emergence of real-life applications based on these efforts. This work has been driven, in part, by the development of new thin film growth techniques and the resulting access to high-quality materials for further study. In general, the field of functional oxide materials has experienced unprecedented growth during the past decades in terms of the discovery of new materials systems and physical phenomena, advances in characterization, and development of deeper understanding of the fundamental properties and how to control these properties through sys-

tematic changes in crystal chemistry (i.e. doping or alloying), strain, and other variables. Perhaps the most interesting recent manifestation of the complex and rich diversity of physical phenomena is the emergence of coupled behavior, in which the lattice, orbital, spin, and charge degrees of freedom are coupled through either quantum mechanics or through engineering design of artificial heterostructures. Of course, such coupling between phenomena is not necessarily new. Piezoelectrics exhibit coupling between mechanics and electrical degrees of freedom and ferromagnetic shape memory alloys exhibit coupling between magnetism and mechanics. But in the last decade, renewed interest in the potential of coupling between the spin and charge degrees of freedom has fascinated researchers and engineers not only from a fundamental perspective, but from an applied direction as well. Imagine a world in which one can control and manipulate magnetism with electric fields (which are intrinsically much easier to use in an actual device, especially in small dimensions, and can potentially provide routes to lower power/energy consumption in systems), thus eliminating currents and magnetic fields.

\* Corresponding author.

E-mail address: [lwmartin@illinois.edu](mailto:lwmartin@illinois.edu) (L.W. Martin).

Creating novel materials and combinations of materials is thus a critical component that enables the exploration of such fascinating phenomena. The power of advanced materials synthesis has been demonstrated in a large number of instances; for example, semiconductor epitaxy has led not only to a large number of technologies, also to several Nobel prizes. Researchers in oxide science have taken a page out of the semiconductor lexicon and consequently, materials synthesis plays a critical role in enabling the study of such novel materials. In this paper, the recent advances in the growth and characterization of multiferroic and magnetoelectric oxide materials (in particular the model multiferroic  $\text{BiFeO}_3$ ) and the interplay between synthesis, theory, and experimental probes will be reviewed. We will summarize with a look to the future of complex oxide materials with special attention given to possible areas of impact for future technologies.

## 2. The crystal chemistry of complex oxides

The general field of metal oxide materials has been the focus of much study because of the broad range of structures, properties, and exciting phenomena present in these materials [1,2]. The perovskite structure, which has the chemical formula  $\text{ABO}_3$  (i.e.  $\text{CaTiO}_3$ ,  $\text{SrRuO}_3$ ,  $\text{BiFeO}_3$ ), is made up of corner-sharing octahedra with the A-cation coordinated with twelve oxygen ions and the B-cation with six. The structure can easily accommodate a wide range of valence states on both the A- and B-sites (i.e.  $\text{A}^{+1}\text{B}^{+5}\text{O}_3$ ,  $\text{A}^{+2}\text{B}^{+4}\text{O}_3$ ,  $\text{A}^{+3}\text{B}^{+3}\text{O}_3$ ) and can exhibit complex defect chemistry (including accommodation of a few percentage of cation non-stoichiometry, large concentrations of oxygen vacancies, and exotic charge accommodation modes ranging from disproportionation to cation ordering and beyond) that maintains charge balance in the structure [3]. One of the most interesting aspects of complex oxides is our ability to engineer or tune their physical properties simply by replacing, substituting, or varying the ratio of the cationic species that are located at the A- and B-sites of the structure. Selection of the appropriate alloying species (chosen to have different formal valence, ionic radius, etc.) can dramatically impact the structural, electronic, magnetic, polar, etc. properties of these materials. In the end, the electronic structure and coordination chemistry of the cationic species control the fundamental physical phenomena manifested in these materials – producing phases that are insulators, metals, superconductors, ion conductors, possess polar distortions and electromechanical responses, magnetic order, and beyond.

The in-depth work in this field has produced a number of design algorithms that allow one to fundamentally manipulate the properties in these perovskite phases and provide guidelines by which one can engineer their properties. As an example, let us consider the case of the prototypical perovskite  $\text{SrTiO}_3$ , which is a good insulator as a consequence of the closed shell electronic structure of both Sr (2+) and Ti (4+ and  $d^0$ ). From a band perspective, the

valence band (predominantly oxygen 2p in character) is filled while the conduction band (predominantly Ti 3d in character) is empty. Simply changing the A-site cation from Sr to La, however, makes a dramatic difference in the electronic structure as well as in the transport properties. In  $\text{LaTiO}_3$ , the Ti is in the 3+ oxidation state and thus in a formal sense has a  $d^1$  electronic structure. As such, it is expected to be a good electrical conductor; however, the reality is something dramatically different.  $\text{LaTiO}_3$  is actually a very good insulator; a so-called Mott insulator [4]. This insulating behavior arises due to the interplay between the kinetic energy of the electron and Coulombic repulsion effects at the atomic scale. In mixed A-site compounds (i.e.  $\text{Sr}_{1-x}\text{La}_x\text{TiO}_3$ ), these two terms trade off one another and the manifested transport properties are the result of this competition. Such materials exhibit strong (sometimes colossal) changes in their transport properties under external thermodynamic stimuli (i.e. temperature, magnetic field, electric field, chemical potential, etc.). Taking this one step further, if one were to take the  $\text{LaTiO}_3$  structure and change the cation at the B-site (the transition metal site), for instance by replacing the Ti with Mn, then one will obtain the antiferromagnetic insulator (insulating for the same reason as for  $\text{LaTiO}_3$ )  $\text{LaMnO}_3$ . There are a number of exquisite treatises on the nature of electronic conduction in oxides (see, for example, Refs. [4,5]) and so we will not elaborate further on this subject here, except to note that the entire evolution of the physics and chemistry of these materials and their implementation into next-generation technologies are dependent on the complex interplay between the cationic stereochemistry, electronic structure, and the interactions among them.

Among the most important aspects in understanding any class of materials is understanding the role of and how to control point defects in materials. In traditional semiconductor systems this control meant mitigation of defects so that one can achieve the true intrinsic electronic properties desired. The study of defects in oxides has a long and rich history. From fast ionic conduction in non-stoichiometric oxides [6] to superconductivity in hole-doped cuprates [7–9] to colossal magnetoresistance in alloyed manganites [10], defects can be essential in defining the properties and performance of oxide materials. Additionally, the multi-component oxide systems, such as the perovskites, are susceptible to complex defect structure development, including compensating densities of cationic vacancies, oxygen vacancies, and the formation of defect complexes (i.e. clusters of defects that exhibit different energetics and behavior from single point defects). For an in-depth review of defects in oxide materials the reader is directed to Refs. [3,11].

## 3. Multiferroism and magnetoelectricity

A hallmark of perovskites is the large variety of functional responses such as ferroelectricity, piezoelectricity, pyroelectricity, ferromagnetism, antiferromagnetism, etc.,

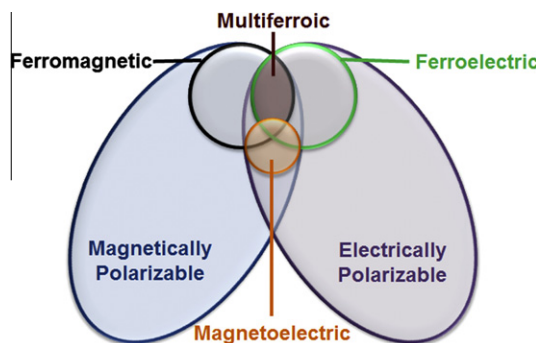


Fig. 1. Relationship between multiferroic and magnetoelectric materials, illustrating the requirements to achieve both in a material (adapted from Ref. [14]).

that form the underpinnings for both advanced technologies (such as ferroelectric nonvolatile memories, SONAR, transformers, etc.) and a wealth of basic science (for example in the colossal magnetoresistant (CMR) manganites). Such a broad range of responses can be enabled within a framework of the oxygen coordination octahedron, by simply changing the cationic occupations of the A- and B-sites. The interplay between the electronic and ionic structure of the cations at the A- and B-sites as well as their ionic sizes, leads to the rich diversity of structural derivatives of the basic simple cubic structure, manifesting in the many types of physical responses. Over the past several years, the exploration of these individual functional responses has evolved into the exploration of coupled order, namely the existence of multiple order parameters, as exemplified by multiferroics. From the investigation of bulk single crystals to novel characterization techniques that probe order parameters, coupling, and spin dynamics this is truly a diverse field, rich with experimental and theoretical complexity. By definition, a single phase multiferroic [12] is a material that simultaneously possesses two or more of the so-called “ferroic” order parameters – such as ferroelectricity, ferromagnetism, and ferroelasticity. Magnetoelectric coupling typically refers to the linear magnetoelectric effect manifested as an induction of magnetization by an electric field or polarization by a magnetic field [13]. The overlap required of ferroic materials to be classified as multiferroic is shown schematically in Fig. 1 [14]. Only a small subgroup of all magnetically and electrically polarizable

materials are either ferromagnetic or ferroelectric and fewer still simultaneously exhibit both order parameters. The ultimate goal for device functionality would be a single phase multiferroic with strong coupling between ferroelectric and ferromagnetic order parameters, enabling simple control over the magnetic nature of the material with an applied electric field at room temperature. Some possible pathways to multiferroic behavior are presented in Table 1.

### 3.1. The model multiferroic, $\text{BiFeO}_3$

There are several pathways available to create coupled order parameters; these are summarized in recent reviews [15,16]. In this review, we will focus specifically on the  $\text{BiFeO}_3$  system, since this is essentially the only single-phase multiferroic that simultaneously possesses both magnetic and ferroelectric order at and above room temperature – prompting unprecedented research and study by the multiferroics community. The perovskite  $\text{BiFeO}_3$  was first produced in the late 1950s [17] and many of the early studies were focused on the same concepts important today – the potential for magnetoelectric coupling [18]. Throughout the 1960s and 1970s much controversy surrounded the true physical and structural properties of  $\text{BiFeO}_3$ , but as early as the 1960s it was suspected to be an antiferromagnetic, ferroelectric multiferroic [19,20]. The true ferroelectric nature of  $\text{BiFeO}_3$ , however, remained somewhat in question until ferroelectric measurements made at 77 K in 1970 [20] revealed a spontaneous polarization of  $\sim 6.1 \mu\text{C cm}^{-2}$  along the  $111$ -direction, consistent with the rhombohedral polar space group  $R\bar{3}c$  determined from single crystal X-ray diffraction [21] and neutron diffraction studies [22]. These findings were confirmed by detailed structural characterization of ferroelectric/ferroelastic monodomain single crystal samples [18]. The structure of  $\text{BiFeO}_3$  can be characterized by two distorted perovskite blocks connected along their body diagonal or the pseudocubic  $\langle 111 \rangle$ , to build a rhombohedral unit cell (Fig. 2a) [23]. In this structure the two oxygen octahedra of the cells connected along the  $\langle 111 \rangle$  are rotated clockwise and counterclockwise around the  $\langle 111 \rangle$  by  $\pm 13.8(3)^\circ$  and the Fe ion is shifted by  $0.135 \text{ \AA}$  along the same axis away from the oxygen octahedron center position. Such large spontaneous distortions should normally be accompanied

Table 1

Summary of pathways to multiferroic order in materials including various Types I and II routes and prototypical materials.

	Pathway to	Mechanism for multiferroism	Examples
Type I	A-site driven	Stereochemical activity of A-site lone pair gives rise to ferroelectricity and magnetism arises from B-site cation	$\text{BiFeO}_3$ , $\text{BiMnO}_3$
	Geometrically driven	Long-range dipole-dipole interactions and oxygen rotations drive the system towards a stable ferroelectric state	$\text{YMnO}_3$ , $\text{BaNiF}_4$
	Charge ordering	Non-centrosymmetric charge ordering arrangements result in ferroelectricity in magnetic materials	$\text{LuFe}_2\text{O}_4$
Type II	Magnetic ordering	Ferroelectricity is induced by the formation of a symmetry-lowering magnetic ground state that lacks inversion symmetry	$\text{TbMnO}_3$ , $\text{DyMnO}_3$ , $\text{TbMn}_2\text{O}_4$

by large spontaneous polarizations as well; however, this did not seem to cause much consternation in the research community, since magnetism in this system is quite exotic and thus captured a lot of interest.

During the 1980s, the magnetic structure of  $\text{BiFeO}_3$  was studied in detail. Early studies indicated that  $\text{BiFeO}_3$  was a G-type antiferromagnet (G-type antiferromagnetic order is shown schematically in Fig. 2d) with a Néel temperature of  $\sim 673$  K [24] and possessed a cycloidal spin structure with a period of  $\sim 620$  Å [25]. This spin structure was found to be incommensurate with the structural lattice and was superimposed on the antiferromagnetic order. It was also noted that if the moments were oriented perpendicular to the  $\langle 111 \rangle$ -polarization direction the symmetry also permits a small canting of the moments in the structure, resulting in a weak canted ferromagnetic moment of the Dzyaloshinskii–Moriya type (Fig. 2d) [26,27].

In 2003 a paper focusing on the growth and properties of thin films of  $\text{BiFeO}_3$  spawned a dramatic increase in the study of  $\text{BiFeO}_3$  thin films that continues to the present day. The paper reported enhancements of polarization and related properties in heteroepitaxially constrained thin films of  $\text{BiFeO}_3$  [28]. Structural analysis of the films suggested differences between films (with a monoclinic structure) and bulk single crystals (with a rhombohedral structure) as well as enhancement of the polarization up to  $\sim 90 \mu\text{C cm}^{-2}$  at room temperature and enhanced thickness-dependent magnetism compared to bulk samples. It is now clear that the high values of polarization observed actually represented the intrinsic polarization of  $\text{BiFeO}_3$ . Limitations in the quality of bulk crystals had kept researchers from observing such high polarization values until much later in bulk samples [29]. A series of detailed first principles calculations methods helped shed light on the findings of Ref. [28]. Calculations of the spontaneous polarization in  $\text{BiFeO}_3$  suggested a value between 90 and  $100 \mu\text{C cm}^{-2}$  (consistent with those measured in 2003) [30] that have since been confirmed by many other experimental reports. Other theoretical treatments attempted to

understand the nature of magnetism and coupling between order parameters in  $\text{BiFeO}_3$ . Such calculations confirmed the possibility of weak ferromagnetism arising from a canting of the antiferromagnetic moments in  $\text{BiFeO}_3$ . The canting angle was calculated to be  $\sim 1^\circ$  and would result in a small, but measurable, magnetization of  $\sim 0.05 \mu_B$  per unit cell [31]. It was also found that the magnetization should be confined to an energetically degenerate, easy  $\{111\}$ , perpendicular to the spontaneous polarization direction in  $\text{BiFeO}_3$ . These same calculations further discussed the connection of the weak ferromagnetism and the structure (and therefore ferroelectric nature) of  $\text{BiFeO}_3$ . This allowed the extraction of three conditions necessary to achieve electric-field-induced magnetization reversal: (i) the rotational and polar distortions must be coupled; (ii) the degeneracy between different configurations of polarization and magnetization alignment must be broken; (iii) there must be only one easy magnetization axis in the  $\{111\}$  which could be easily achieved by straining the material [31].

Nonetheless, the true nature of magnetism in thin film  $\text{BiFeO}_3$  continues to be a contentious subject. The work of Wang et al. presented an anomalously large value of magnetic moment (of the order of  $70 \text{ emu cm}^{-3}$ ) [28], which is significantly higher than the expected canted moment of  $\sim 8 \text{ emu cm}^{-3}$ . There have been several studies aimed at clarifying the origins of this anomalous magnetism. Eerenstein et al. [32] proposed that the excess magnetism was associated with magnetic second phases (such as  $\gamma\text{-Fe}_2\text{O}_3$ ); this was supported by the studies of Béa et al. [33], who showed that  $\text{BiFeO}_3$  films, when grown under highly reducing conditions (for example under oxygen pressures lower than  $1 \times 10^{-3}$  Torr) showed enhanced magnetism as a consequence of the formation of magnetic second phases. It is, however, important to note that low oxygen pressure during growth is not the cause for the enhanced moment in the 2003 report by Wang et al., where films were grown in oxygen pressures between 100 and 200 mTorr and cooled in 760 Torr, rendering formation of such secondary magnetic phases thermodynamically

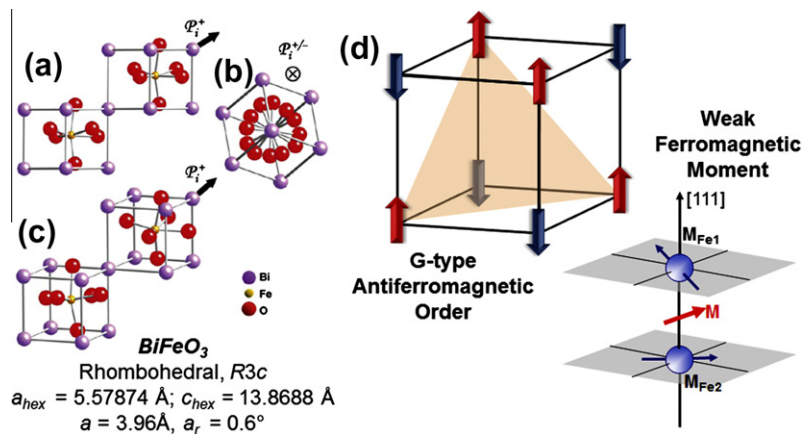


Fig. 2. Structure of  $\text{BiFeO}_3$  shown looking (a) down the pseudocubic-[110], (b) down the pseudocubic-[111] polarization direction, and (c) at a general three-dimensional view of the structure. (d) The magnetic structure of  $\text{BiFeO}_3$  is shown, including G-type antiferromagnetic ordering and the formation of the weak ferromagnetic moment (adapted from Ref. [23]).

unlikely, and there was no evidence (despite extensive study of samples with X-ray diffraction and transmission electron microscopy techniques) for such second phases. Furthermore, subsequent X-ray magnetic circular dichroism studies supported the assertion that this magnetism is not from a magnetic  $\gamma\text{-Fe}_2\text{O}_3$  impurity phase [34]. To date, contradicting reports – including those of enhanced magnetism in nanoparticles of  $\text{BiFeO}_3$  [35] as well as the observation of samples exhibiting no such enhancement – have been presented. It is thus fair to say that this is an issue that remains unresolved in a rigorous sense.

Today, much progress has been made in understanding the structure, properties, and growth of thin films of  $\text{BiFeO}_3$ . High-quality epitaxial  $\text{BiFeO}_3$  films have been grown via molecular beam epitaxy (MBE) [36,37], pulsed laser deposition [28,38], radio-frequency (RF) sputtering [39,40], metalorganic chemical vapor deposition (MOCVD) [41,42], and chemical solution deposition (CSD) [43] on a wide range of substrates including traditional perovskite oxide substrates (with lattice parameters ranging from 3.86 to 4.01 Å, covering a range from 2.5% compressive strain to 1.3% tensile strain) as well as Si [38,44] and GaN [45]. This work has shown that high-quality films, like those shown in Fig. 3, can be routinely produced. Typical X-ray diffraction  $\theta$ - $2\theta$  measurements (Fig. 3a) illustrate the state-of-the-art in terms of high-quality, fully epitaxial, single-phase films (data here are for a  $\text{BiFeO}_3/\text{SrRuO}_3/\text{SrTiO}_3$  (001) heterostructure). Detailed X-ray diffraction analysis has shown that films possess a monoclinic distortion of the bulk rhombohedral structure over a wide range of thicknesses, but the true structure of very thin films ( $<15$  nm) remains unclear [46]. The quality of such heterostructures can be probed further by transmission electron microscopy (TEM) (Fig. 3b) [47]. TEM imaging reveals films that are uniform over large areas and with the use of high-resolution TEM we can examine the atomically abrupt, smooth, and coherent interface between  $\text{BiFeO}_3$  and a commonly used bottom electrode material  $\text{SrRuO}_3$ . Detailed studies of such epitaxial oxide interfaces reveal

that the rules of semiconductor heteroepitaxy with regard to relaxation of misfit strain through the formation of interface dislocations are valid for oxides as well. In this specific example, the lattice mismatch between  $\text{SrRuO}_3$  and  $\text{BiFeO}_3$  is  $\sim 0.3\%$  and thus pseudomorphic growth is possible for thicknesses of  $\sim 30$  nm. Prior work has shown, for example, that the density of misfit dislocations does indeed scale with the lattice mismatch between the two layers [48].

### 3.2. Evolution of antiferromagnetism in $\text{BiFeO}_3$ thin films

As was discussed previously, the structure of  $\text{BiFeO}_3$  can be characterized by two distorted perovskite blocks connected along their body diagonal or the pseudocubic  $\langle 111 \rangle$  to build a rhombohedral unit cell.  $\text{BiFeO}_3$  is also a G-type antiferromagnet with the moments confined to a plane perpendicular to the  $\langle 111 \rangle$ -polarization directions and possesses symmetry that permits a small canting of the moments in the structure, resulting in a weak ferromagnetic moment of the Dzyaloshinskii–Moriya type [26,27]. Ederer and Spaldin suggested that only one easy magnetization axis in the energetically degenerate  $111$ -plane might be selected when the crystal is strained [31]. The application of the appropriate strain (not defined in this initial work) would likely break the degeneracy between the eight available orientation variants possible in this system, thereby lowering the energy of a single direction in the plane. Thus, one critical question concerning magnetism in multiferroics such as  $\text{BiFeO}_3$  that is of both fundamental and technological importance is how this order parameter develops with strain and size effects. Using angle- and temperature-dependent X-ray linear dichroism measurements and photoemission spectromicroscopy, Holcomb et al. [49] discovered that the antiferromagnetic order in  $\text{BiFeO}_3$  does evolve and changes systematically as a function of thickness and strain. Lattice mismatch induced strain is found to break the easy-plane magnetic symmetry of the bulk and leads to an easy axis of magnetization which can be

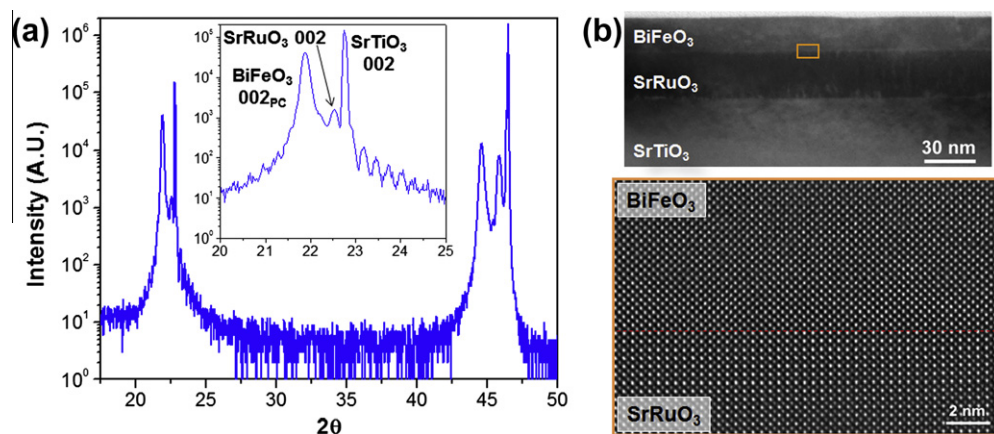


Fig. 3. (a) X-ray diffraction results from a fully epitaxial, single-phase  $\text{BiFeO}_3/\text{SrRuO}_3/\text{SrTiO}_3$  (001) heterostructure (courtesy of A.R. Damodaran and L.W. Martin). (b) Low-resolution (top) and high-resolution (bottom) transmission electron microscopy images of  $\text{BiFeO}_3/\text{SrRuO}_3/\text{SrTiO}_3$  (001) heterostructure (adapted from Ref. [47]).

controlled via the sign of the strain – 110-type for tensile strain and 112-type for compressive strain. Such an understanding of the evolution of magnetic structure and the ability to manipulate the magnetism in this model multiferroic have significant implications for eventual utilization in applications. In particular, researchers are interested in utilizing the electric field control of antiferromagnetism in materials like BiFeO<sub>3</sub> to enable electric field tunable magnetism for memories, logics, sensing and more.

### 3.3. Role of domain walls in BiFeO<sub>3</sub>

Recent observations are helping to answer questions surrounding the wide spectrum of magnetic responses observed in BiFeO<sub>3</sub> thin films. There is now a growing consensus that epitaxial films (with a thickness less than ~100 nm) are highly strained and thus the crystal structure is more akin to a monoclinic phase rather than the bulk rhombohedral structure. In films >100 nm, depending on the film–substrate lattice mismatch, films can relax to the bulk-like distorted rhombohedral structure and give rise to magnetic properties consistent with the weak canting of the antiferromagnetic moments. Furthermore, a systematic dependence of the ferroelectric domain structure in the film as a function of the growth rate has been observed [50]. Films grown very slowly (for example by MBE, laser MBE, or off-axis sputtering) exhibit a classical stripe-like domain structure that is similar to ferroelastic domains in tetragonal Pb(Zr<sub>x</sub>Ti<sub>1-x</sub>)O<sub>3</sub> films. Due to symmetry considerations, two sets of such twins are observed. These twins are made up of 71° ferroelastic domain walls, which form on the {101}-type planes (which is a symmetry plane). In contrast, if the films are grown rapidly (as was done in the original work of Wang et al. [28]) the domain structure is dramatically different (likely arising from a change in the growth mechanism from a step-flow or layer-by-layer process to an island growth process). It now resembles a mosaic-like ensemble that consists of a dense distribution of 71°, 109°, and 180° domain walls. It should be noted that 109° domain walls form on {001}-type planes (which is not a symmetry plane for this structure). Preliminary measurements reveal a systematic difference in magnetic moment between samples possessing different types and distributions of domain walls. The work of Martin et al. [50] suggests that such domain walls could play a key role in many observations of enhanced magnetic moment in BiFeO<sub>3</sub> thin films.

This hypothesis emerges from the work of Přívratská and Janovec [51,52], where detailed symmetry analyses were used to arrive at the conclusion that magnetoelectric coupling could lead to the appearance of a net magnetization in the middle of antiferromagnetic domain walls. Their idea was that domain walls represent a special kind of inhomogeneity where a lowering of the translation symmetry to two dimensions confines the appearance of new effects to a layer – the symmetry of the layer can be described by a so-called layer group. Such layer groups exclude some sym-

metry elements that may exist in the bulk of a domain (i.e. rotation and inversion axes that are not perpendicular or parallel to the domain wall) or may allow for invariance under operations that interchange domains on the two sides of the wall. Such operations cannot exist in the bulk of domains and thus result in an enhancement of symmetry. Thus the symmetry difference between the bulk of a domain and the domain wall is generally not a simple symmetry lowering and thus not only can induce an appearance of new effects in the domain wall that do not exist in the bulk of a domain, but also can result in the disappearance of some properties that exist in the bulk of the domain. The work of Janovec and colleagues focused on the possible appearance of spontaneously magnetized domain walls joining antiferromagnetic domains, especially in multiferroic/magnetoelectric crystals, while other prior studies suggested the possibility of electric polarization in domain walls in magnetically ordered crystals. [53] In the end, this work showed that this effect is allowed for materials with the *R3c* space group (i.e. that observed for BiFeO<sub>3</sub>). Although this analysis raises the possibility of an enhanced moment, the group-symmetry arguments do not allow for any quantitative estimate of that moment.

The idea that novel properties could occur at domain walls in materials presented by Přívratská and Janovec is part of a larger field of study of the morphology and properties of domains and their walls that has taken place over the last 50 years, with increasing recent attention given to the study novel functionality at domain walls [54–56]. For instance, recent work has demonstrated that spin rotations across ferromagnetic domain walls in insulating ferromagnets can induce a local polarization in the walls of otherwise non-polar materials (incommensurate magnetic ordering results from competing exchange interactions and the resulting spin density wave can induce a Lifshitz invariant coupling that induces a uniform electric polarization that breaks the inversion symmetry) [16,56], preferential doping along domain walls has been reported to induce two-dimensional superconductivity in WO<sub>3-x</sub> [57] and enhanced resistivity in phosphates [58], while in paraelectric (non-polar) SrTiO<sub>3</sub> the ferroelastic domain walls appear to be ferroelectrically polarized [59]. Taking this idea one step further, Daraktchiev et al. [60,61] have proposed a thermodynamic (Landau-type) model with the aim of quantitatively estimating whether the walls in BiFeO<sub>3</sub> can be magnetic and if so, to what extent they might contribute to the observed enhancement of magnetization in ultrathin films. One can develop a simple thermodynamic potential incorporating two order parameters expanded up to *P*<sup>6</sup> and *M*<sup>6</sup> terms (the transitions in BiFeO<sub>3</sub> are found experimentally to be first order, and the low-symmetry ( $\pm P_0, 0$ ) phase is described here) with biquadratic coupling between the two order parameters (biquadratic coupling is always allowed by symmetry, and therefore always present in any system with two order parameters). The authors also note that there is no published data on the Landau coefficients for BiFeO<sub>3</sub>, no esti-

mates of domain-wall magnetization, and no analytical expression of domain wall magnetization as a function of domain-wall thickness, coupling, and the all-important Landau coefficients (which determine the accuracy of such phenomenological models). The authors recommend rigorous measurement of the Landau coefficients for  $\text{BiFeO}_3$  and suggest that this could greatly increase our understanding of these and other topics.

Regardless, when one goes from  $+P$  to  $-P$ , it is energetically more favorable for the domain wall energy trajectory not to go through the center of the landscape ( $P = 0$ ,  $M = 0$ ), but to take a diversion through the saddle points at  $M_0 \neq 0$ , thus giving rise to a finite magnetization (Fig. 4). The absolute values of the magnetic moment at the domain wall will depend on the values of the Landau coefficients as well as the boundary conditions imposed on the system, namely whether the material is magnetically ordered or not. Analysis of the phase space of this thermodynamic potential shows that it is possible for the net magnetization to appear in the middle of ferroelectric walls, even when the domains themselves are not ferromagnetic (Fig. 4b). The authors of this model note, however, that it is presently only a “conceptual model” which does not take into account the exact symmetry of  $\text{BiFeO}_3$ , so it cannot yet quantitatively estimate how much domain walls can contribute to the magnetization. The exact theory of magnetoelectric coupling at the domain walls of  $\text{BiFeO}_3$  also remains to be formulated.

Recently, a holistic picture of the connection between processing, structure, and properties has brought to light the role of magnetism at ferroelectric domain walls in determining the magnetic properties in  $\text{BiFeO}_3$  thin films. By controlling domain structures through epitaxial growth constraints and probing these domain walls with magneto-transport and high-resolution transmission electron microscopy, He et al. [62] have demonstrated that certain types of ferroelectric domain walls (i.e.  $109^\circ$  walls) can possess exotic magnetic properties in  $\text{BiFeO}_3$ . Building off the

work of Martin et al. [50], they were able to demonstrate that samples possessing  $109^\circ$  domain walls show significantly enhanced circular dichroism that is consistent with collective magnetic correlations, while samples with only  $71^\circ$  domain walls show no measurable circular dichroism. In summary, it appears that certain domain walls can give rise to enhanced magnetic behavior in  $\text{BiFeO}_3$  thin films.

Seidel et al. [63] undertook a detailed scanning probe-based study of domain walls in  $\text{BiFeO}_3$  and discovered a new and previously unanticipated finding: the observation of room temperature electronic conductivity at certain ferroelectric domain walls. The origin of the observed conductivity was explored using high-resolution transmission electron microscopy and first-principles density functional computations. The results showed that domain walls in a multiferroic ferroelectric, such as  $\text{BiFeO}_3$ , can exhibit unusual electronic transport behavior on a local scale that is quite different from that in the bulk of the material. Using a model (110)-oriented  $\text{BiFeO}_3/\text{SrRuO}_3/\text{SrTiO}_3$  heterostructure with a smooth surface (Fig. 5a), the researchers were able to switch the  $\text{BiFeO}_3$  material in such a way that enabled them to create all the different types of domain walls possible in  $\text{BiFeO}_3$  (i.e.  $71^\circ$ ,  $109^\circ$ , and  $180^\circ$  domain walls) in a local region (Fig. 5b and c). Conducting atomic force microscopy (c-AFM) measurements (Fig. 5d) revealed conduction at  $109^\circ$  and  $180^\circ$  domain walls. Detailed high-resolution transmission electron microscopy studies (Fig. 5e) revealed that this conductivity was, in part, structurally induced and can be activated and controlled on the scale of the domain wall width –  $\sim 2$  nm in  $\text{BiFeO}_3$ . From the combined study of conductivity measurements, electron microscopy analysis, and density functional theory calculations, two possible mechanisms for the observed conductivity at the domain walls have been suggested: (1) an increased carrier density as a consequence of the formation of an electrostatic potential step at the wall; and/or (2) a decrease in the band gap within the wall and corresponding reduction in band offset with the c-AFM tip. It was

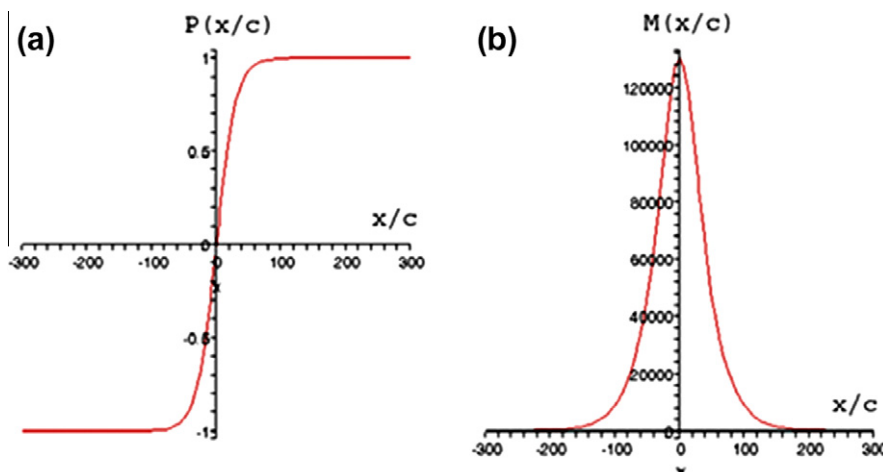


Fig. 4. Shape of ferroelectric polarization and magnetism across a domain wall in  $\text{BiFeO}_3$ . (a) Ferroelectric polarization goes to zero at the center of the domain wall. (b) A net magnetization appears at the center of the domain wall, even though the domains themselves do not possess a net moment (adapted from Refs. [60,61]).

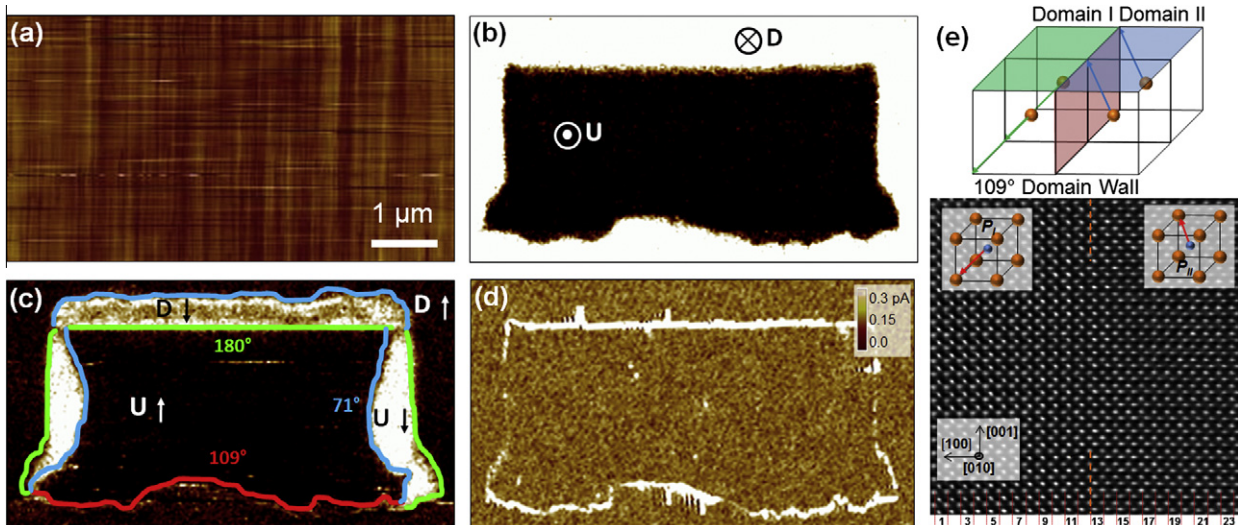


Fig. 5. Conduction at domain walls in  $\text{BiFeO}_3$ . (a) Topographic image of the surface of a model  $\text{BiFeO}_3/\text{SrRuO}_3/\text{SrTiO}_3$  (110) sample as image via atomic force microscopy. Corresponding out-of-plane (b) and in-plane (c) piezoresponse force microscopy images of a switch portion of the same film. Domain wall types and locations are labeled. (d) Conducting-atomic force microscopy image of switched portion of the film reveals certain types (name 109° and 180° domain walls) that conduct. (e) Schematic illustration of a 109° domain wall and corresponding high-resolution transmission electron microscopy image of a 109° domain wall. Analysis reveals the presence of a net polarization perpendicular to the domain wall and a change in the local structure at the domain wall – both of which could give rise to enhanced conduction (adapted from Ref. [63]).

found that the normal component of the polarization showed a small increase in the vicinity of the domain wall. Calculations indicated that this small change in the normal component of the polarization across these domain walls could lead to a step in the electrostatic potential (planar and macroscopically averaged) of 0.15–0.18 eV across the domain wall, similar to a step computed previously for 90° domain walls in  $\text{PbTiO}_3$  [64]. Such a potential step should enhance the electrical conductivity by causing carriers in the material to accumulate at the domain wall to screen the polarization discontinuity. Additionally, the change in the structure (trending towards higher symmetry) could also result in a narrowing of the band gap for this material. It was noted that both situations are the result of the same structural changes at the wall and both may, in principle, be acting simultaneously, since they are not mutually exclusive.

#### 3.4. Magnetoelectric coupling in $\text{BiFeO}_3$

Although many researchers anticipated strong magnetoelectric coupling in  $\text{BiFeO}_3$ , until the first evidence for this coupling in 2003 there was no definitive proof. Three years after this first evidence, a detailed report was published in which researchers observed the first visual evidence for electrical control of antiferromagnetic domain structures in a single phase multiferroic at room temperature. By combining X-ray photoemission electron microscopy (PEEM) imaging of antiferromagnetic domains (Fig. 6a and b) and piezoresponse force microscopy (PFM) imaging of ferroelectric domains (Fig. 6c and d), they were able to directly observe changes in the nature of the antiferromagnetic domain structure in  $\text{BiFeO}_3$  with application of an applied electric field (Fig. 6e) [65]. This research showed

that the ferroelastic switching events (i.e. 71° and 109°) resulted in a corresponding rotation of the magnetization plane in  $\text{BiFeO}_3$  (Fig. 6f) and has paved the way for further study of this material in attempts to gain room temperature control of ferromagnetism (to be discussed in detail later) and has since been confirmed by neutron diffraction experiments in bulk  $\text{BiFeO}_3$  as well [66].

#### 3.5. Horizontal multilayer heterostructures

An alternative approach to obtain a magnetoelectric effect is through multilayered heterostructures. Great strides have been made in the area of composite magnetoelectric systems. These systems operate by coupling the magnetic and electric properties between two materials, generally a ferroelectric material and a ferrimagnetic material, via the lattice (i.e. piezomagnetism couples to piezoelectricity). An applied electric field creates a piezoelectric strain in the ferroelectric, which produces a corresponding strain in the ferrimagnetic material and a subsequent piezomagnetic change in magnetization or the magnetic anisotropy. Work started in the field several decades ago using bulk composites, although experimental magnetoelectric voltage coefficients were far below those calculated theoretically [67]. In the 1990s theoretical calculations showed the possibility for strong magnetoelectric coupling in a multilayer (2–2) configuration; an ideal structure to be examined by the burgeoning field of complex oxide thin-film growth [68]. In this spirit, researchers experimentally tested a number of materials in a laminate thick-film geometry, including ferroelectrics such as  $\text{Pb}(\text{Zr}_x,\text{Ti}_{1-x})\text{O}_3$  [69–74],  $\text{Pb}(\text{Mg}_{0.33}\text{Nb}_{0.67})\text{O}_3-\text{PbTiO}_3$  (PMN–PT) [75], and ferrimagnets such as  $\text{TbDyFe}_2$  (Terfenol-D) [69],  $\text{NiFe}_2\text{O}_4$  [70,72],  $\text{CoFe}_2\text{O}_4$  [74],  $\text{Ni}_{0.8}\text{Zn}_{0.2}\text{Fe}_2\text{O}_4$  [71],  $\text{La}_{0.7}\text{Sr}_{0.3}$

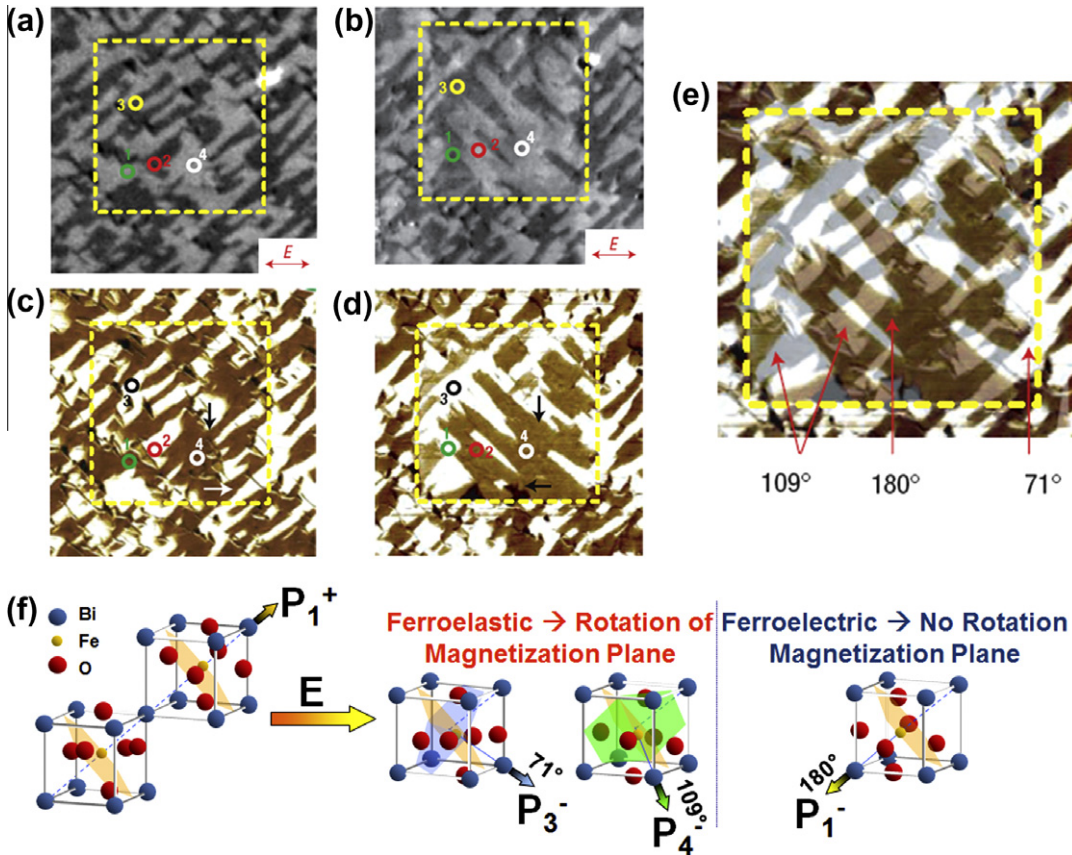


Fig. 6. Determination of strong magnetoelectric coupling in  $\text{BiFeO}_3$ . Photemission electron microscopy (PEEM) images before (a) and after (b) electric field poling. The arrows show the X-ray polarization direction during the measurements. In-plane PFM images before (c) and after (d) electric field poling. The arrows show the direction of the in-plane component of ferroelectric polarization. Regions 1 and 2 (marked with green and red circles, respectively) correspond to  $109^\circ$  ferroelectric switching, whereas 3 (black and yellow circles) and 4 (white circles) correspond to  $71^\circ$  and  $180^\circ$  switching, respectively. In regions 1 and 2 the PEEM contrast reverses after electrical poling. (e) A superposition of in-plane PFM scans shown in (c and d) used to identify the different switching mechanisms that appear with different colors and are labeled in the figure (adapted from Ref. [65]). (f) Schematic illustration of coupling between ferroelectricity and antiferromagnetism in  $\text{BiFeO}_3$ . Upon electrically switching  $\text{BiFeO}_3$  by the appropriate ferroelastic switching events (i.e.  $71^\circ$  and  $109^\circ$  changes in polarization) a corresponding change in the nature of antiferromagnetism is observed (adapted from Ref. [65]). (For interpretation of the references to color in this figure legend, the reader is referred to the web version of this article.)

$\text{MnO}_3$  [73],  $\text{La}_{0.7}\text{Ca}_{0.3}\text{MnO}_3$  [73], and others. These experiments showed great promise and magnetoelectric voltage coefficients up to  $\Delta E/\Delta H = 4680 \text{ mV cm}^{-1} \text{ Oe}^{-1}$  have been observed. Work also continued investigating thin-film heterostructures by combining such ferroelectrics as  $\text{Ba}_{0.6}\text{Sr}_{0.4}\text{TiO}_3$ ,  $\text{BaTiO}_3$  [76], and PMN–PT [77] with ferromagnets such as  $\text{Pr}_{0.85}\text{Ca}_{0.15}\text{MnO}_3$  [76] and Tb–Fe/Fe–Co multilayers [77]; however, these attempts were unable to produce magnetoelectric voltage coefficients above a few tens of  $\text{mV cm}^{-1} \text{ Oe}^{-1}$ . Current theories suggest that the in-plane magnetoelectric interface is limiting the magnitude of this coefficient due to the clamping effect of the substrate on the ferroelectric phase [78]. Since the amount of strain that can be imparted by the ferroelectric phase is limited via this in-plane interfacial geometry, the magnetoelectric voltage coefficient can be reduced by up to a factor of five.

### 3.6. Vertical nanostructures

A seminal paper by Zheng et al. [79] showed that magnetoelectric materials could also be fabricated in a nano-

structured columnar fashion (Fig. 7a). By selecting materials that spontaneously separate due to immiscibility, such as spinel and perovskite phases [67], one can create nanostructured phases made of pillars of one material embedded in a matrix of another. Additionally, the large difference in lattice parameters between these phases leads to the formation of pillars with dimensions on the order of 10 nm, ensuring a high interface-to-volume ratio and strong coupling via strain. In this initial paper, researchers reported structures consisting of  $\text{CoFe}_2\text{O}_4$  pillars embedded in a  $\text{BaTiO}_3$  matrix. Such structures were shown to exhibit strong magnetoelectric coupling (Fig. 7b) via changes in magnetization occurring at the ferroelectric Curie temperature of the matrix material. These nanostructures, in which the interface is perpendicular to the substrate, remove the effect of substrate clamping and allow for better strain-induced coupling between the two phases. An explosion of research into alternative material systems followed as the design algorithm proved to be widely applicable to many perovskite–spinel systems. Nanostructured composites with combinations of a number of perovskite

( $\text{BaTiO}_3$  [80],  $\text{PbTiO}_3$  [81],  $\text{Pb}(\text{Zr}_x\text{Ti}_{1-x})\text{O}_3$  [82,83], and  $\text{BiFeO}_3$  [84,85]) and spinel ( $\text{CoFe}_2\text{O}_4$  [82,83],  $\text{NiFe}_2\text{O}_4$  [81,84], and  $\gamma\text{-Fe}_2\text{O}_3$  [85]) or corundum ( $\alpha\text{-Fe}_2\text{O}_3$  [85]) structures have been investigated. Pulsed laser deposition has proven to be a successful growth technique for achieving satisfactory properties in these nanostructured films [80,86,87].

The magnetoelectric coupling coefficients of such materials are often difficult to measure directly, because of issues arising from leakage in the materials. In many cases, the low resistance of the magnetic pillars penetrating through the films or the magnetic matrix limits the ability to probe these properties directly and could limit the efficacy of these vertical nanostructures in devices [88].

Zavaliche et al. [89] showed  $\Delta E/\Delta H = 100 \text{ V cm}^{-1} \text{ Oe}^{-1}$  at room temperature in a system comprising  $\text{CoFe}_2\text{O}_4$  pillars embedded in a  $\text{BiFeO}_3$  matrix. These films were analyzed with scanning probe techniques that utilized both magnetized and conducting tips. Typical surface morphology for such samples is shown in Fig. 7c. Magnetic measurements show the preference of such structures to maintain magnetization along the length of the nanopillars. Magnetic force microscopy scans both before (Fig. 7d) and after electric field poling (Fig. 7e) show that a significant number of  $\text{CoFe}_2\text{O}_4$  pillars switch their magnetic state from a downward direction to an upward direction upon application of an electric field [90]. This work further showed that the magnetization-switching event was non-deterministic and could be improved by applying a small

magnetic field (700 Oe) to the sample. This field is essential to break time reversal symmetry and overcome the degeneracy between the up and down magnetization states. Nonetheless, these structures have been shown to be very versatile and offer an excellent opportunity for electrically controlled magnetic storage.

### 3.7. Phase stability and self-assembled mixed phase nanostructures

Epitaxy presents a powerful pathway to control the phase stability and electronic properties in thin film systems, as has been well demonstrated in semiconductor heteroepitaxy [91]. The  $\text{BiFeO}_3$  system presents a fascinating parallel in terms of how the phase stability in the system evolves with strain (or stress) imposed through heteroepitaxy. Although the structure of  $\text{BiFeO}_3$  had been studied for many years [21,22,18], in 2005 the structural stability of the parent phase had come into question [92,93]. This was followed, in turn, by a number of thin film studies reporting that a tetragonally distorted phase (derived from a structure with  $P4mm$  symmetry,  $a \sim 3.665 \text{ \AA}$ , and  $c \sim 4.655 \text{ \AA}$ ) with a large spontaneous polarization may be possible [92,94,95]. But it was the report of the so-called mixed-phase thin-films possessing tetragonal- and rhombohedral-like phases in complex stripe-like structures that give rise to enhanced electromechanical responses [96] that really launched this field. Zeches et al. observed that the rhombohedral bulk crystal structure of the parent phase

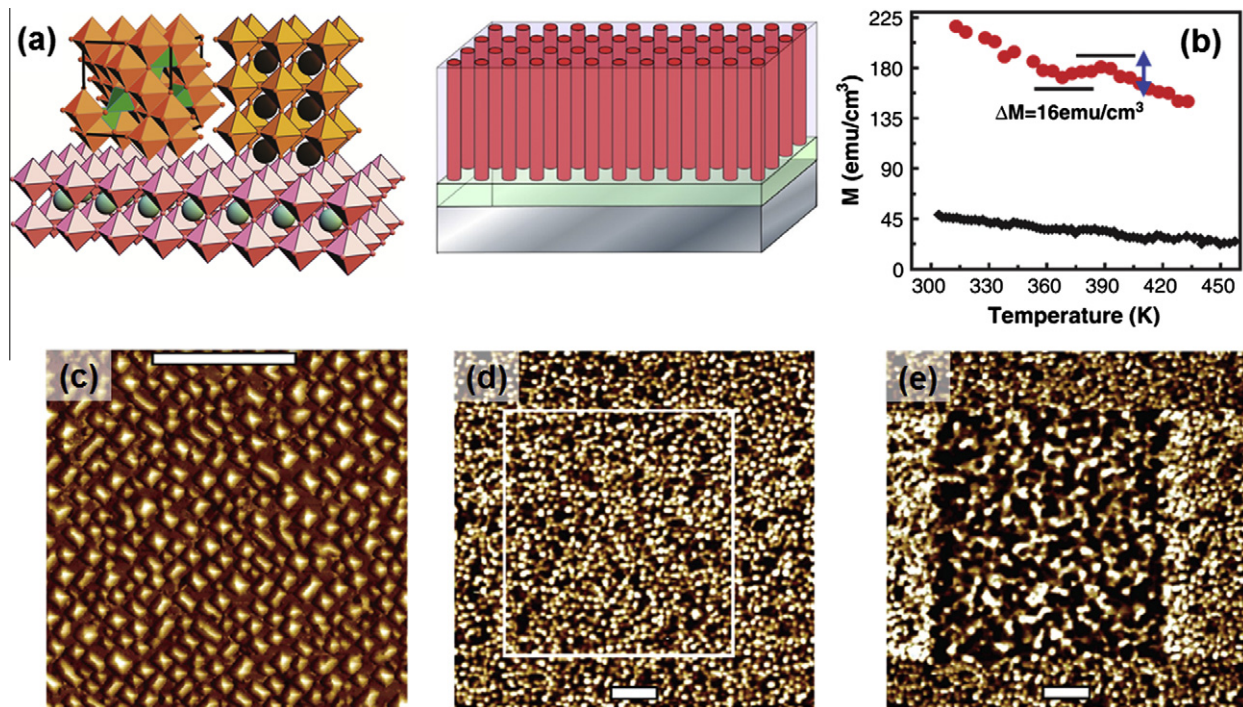


Fig. 7. Multiferroic nanostructures. (a) Schematic illustrations of vertical nanostructure of spinel pillars embedded in a perovskite matrix grown on a perovskite substrate. (b) Magnetization vs. temperature curve measured at 100 Oe, showing a distinct drop in magnetization at the ferroelectric Curie temperature – proof of strong magnetoelectric coupling. (c) Surface topography of a  $\text{CoFe}_2\text{O}_4/\text{BiFeO}_3$  nanostructure as imaged by atomic force microscopy. Magnetic force microscopy scans taken in the same area before (d) and after electrical poling at  $-16 \text{ V}$  (e) (scale bars are  $1 \mu\text{m}$ ) (adapted from Refs. [79,90]).

can be progressively distorted into a monoclinic (and perhaps even a triclinic) structure through in-plane lattice mismatch with the substrate. Ab initio calculations of the role of epitaxial strain clearly demonstrate how it can be used to drive a strain-induced structural change in  $\text{BiFeO}_3$  (Fig. 8a and b). These calculations suggest that at a certain value of epitaxial strain, in the absence of misfit accommodation through dislocation formation, the structure of  $\text{BiFeO}_3$  discontinuously changes from the distorted rhombohedral parent phase structure to a tetragonal (or slightly monoclinically distorted) structure that is characterized by a large  $c/a$  ratio of  $\sim 1.26$ . This “super-tetragonal” structure is distinctly different from the rhombohedral structure in that the coordination of the Fe ion is now five-fold instead of the usual six-fold coordination in the perovskite structure. Direct atomic resolution images of the two phases (Fig. 8c and d), clearly show the difference in the crystal coordination.

Now, an interesting question arises: what happens if one picks a substrate such as  $\text{LaAlO}_3$ , (that has  $\sim 4.5\%$  lattice mismatch with the parent rhombohedral  $\text{BiFeO}_3$  phase) and grows a film in which this epitaxial constraint is partially relaxed? Such experiments (and the corresponding theoretical aspects) have been explored in some detail.

Experimentally, it has been observed that the result is a nanoscale mixed-phase structure, typified by the AFM image and line-trace (Fig. 8e and f, respectively). Fig. 8g is an atomic resolution TEM image of the interface between these two phases and reveals one of the most provocative aspects of the structure. Although there is a large “formal” lattice mismatch between the two phases, the interface appears to be coherent, i.e. it shows no indication for the formation of interphase dislocations. Indeed, this mismatch appears to be accommodated by the gradual deformation of the structure between different phases. In a formal sense, this transformation is termed an isostructural transformation, i.e. one in which the crystal symmetry does not change, but the coordination does. Thus, one can visualize the nanoscale mixed phase ensemble as analogous to the relaxor ferroelectrics or the CMR manganites, both of which exhibit a nanoscale mixture of two phases, and perhaps presents yet another manifestation of a generic “microstructural” design criterion of creating heterophase mixtures with controllable length scales to achieve the desired properties (such as lath martensite in alloy steels, precipitation hardened Al and Ti alloys) [97,98].

Application of dc electric fields to these mixed-phase structures can give rise to large electromechanical

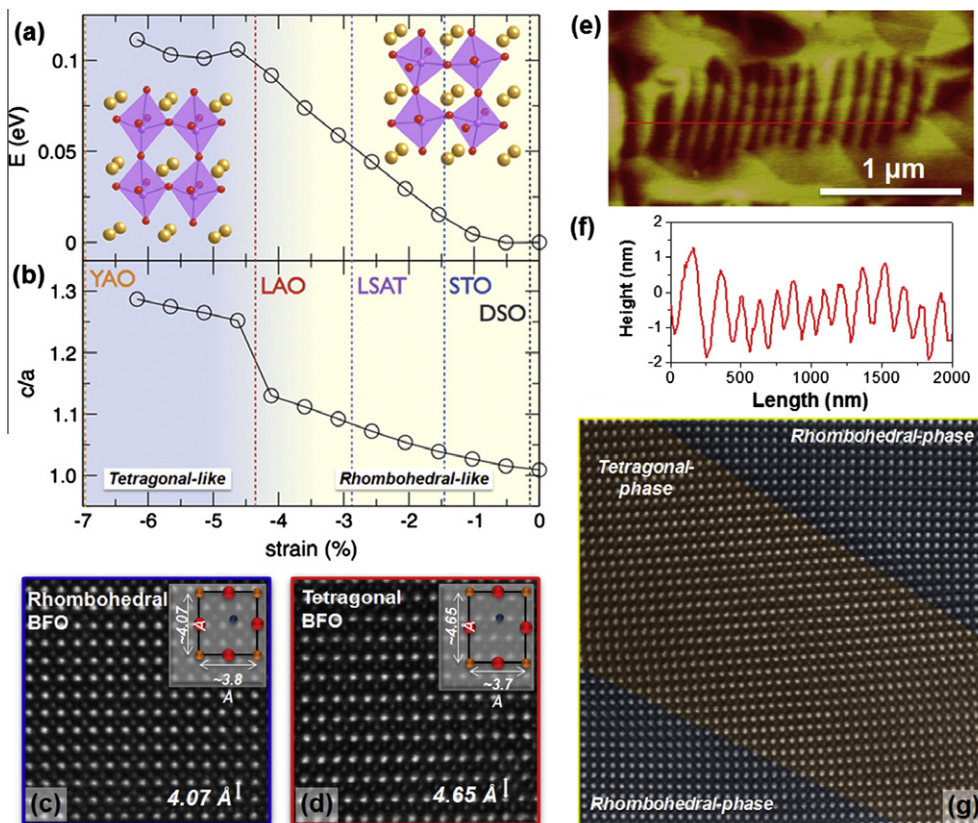


Fig. 8. Strain-induced phase complexity in  $\text{BiFeO}_3$ . First-principle calculations provide information on the strain evolution of (a) the overall energy of the system and (b) the  $c/a$  lattice parameter ratio. High-resolution transmission electron microscopy (HRTEM) reveals the presence of two phases: (c) a monoclinic version of the bulk rhombohedral phase, and (d) high-distorted monoclinic version of a tetragonal structure. These complex phase boundaries manifest themselves on the surface of the sample as imaged via (e) atomic force microscopy and these features correspond to dramatic surface height changes as shown from the line trace (f). (g) HRTEM imaging of boundaries shows a smooth transition between phases (adapted from Ref. [96]).

responses (as large as 4–5%). In situ TEM studies coupled with nanoscale electrical and mechanical probing reveal that such large strains result from moving the boundaries between different phases [99]. Additional studies have shed light on the true nature of these mixed-phase structures and the mechanism for this strong electromechanical response. To begin, since the work by Zeches et al. additional information has come forth about the symmetry of these phases, including the fact that the so-called tetragonal-like phase is actually monoclinically distorted (possessing *Cc*, *Cm*, *Pm*, or *Pc* symmetry) [100–103]. Nonetheless, a thorough understanding of the complex structure of these phase boundaries in  $\text{BiFeO}_3$  remained incomplete.

Using a combination of high-resolution X-ray diffraction and scanning-probe microscopy-based studies, however, Damodaran et al. [104] have uniquely identified and examined the numerous phases present at these phase boundaries and discovered an intermediate monoclinic phase in addition to the previously observed rhombohedral- and tetragonal-like phases. Further analysis has determined that the so-called mixed-phase regions of these films were not mixtures of the rhombohedral- and tetragonal-like phases, but intimate mixtures of a highly distorted monoclinic phase with no evidence for the presence of the rhombohedral-like parent phase. This work also provided a mechanism for the enhanced electromechanical response observed in these films, including how these phases interact at the nanoscale to produce large surface strains. This was obtained by completing detailed local electric-field-dependent switching and capturing both the topography (left

images, Fig. 9) and the out-of-plane orientation of the polarization (right images, Fig. 9) of the sample at a range of electric fields. By navigating the hysteretic nature of electric field response in this material, a number of important features of this system were revealed: (1) the large surface strains (4–5%) occur any time the material transforms from a mixed-phase structure to the highly distorted monoclinic phase, (2) these transformations between these two states are likely reversible, and (3) there are numerous pathways to achieve large electromechanical responses in these materials – including ones that do not need switching of the polar state of the sample. This, in turn, provides a plausible mechanism for the enhanced electromechanical response. The key appears to be the ability to transform between the different phases through a diffusion-less phase transition (in similar fashion to the behavior of a martensitic phase).

A number of additional studies on strain-induced phases have been reported in recent months. This includes a detailed neutron scattering study of a nearly phase-pure film of the highly distorted tetragonal-like phase which confirms antiferromagnetism with largely G-type character and a  $T_N = 324$  K, a minority magnetic phase with C-type character, and suggests that the co-existence of the two magnetic phases and the difference in ordering temperatures from the bulk phase can be explained through simple Fe–O–Fe bond distance considerations [105]. Other reports suggest the possibility of a reversible temperature-induced phase transition at  $\sim 100$  °C in the highly distorted tetragonal-like phase as studied by temperature-dependent

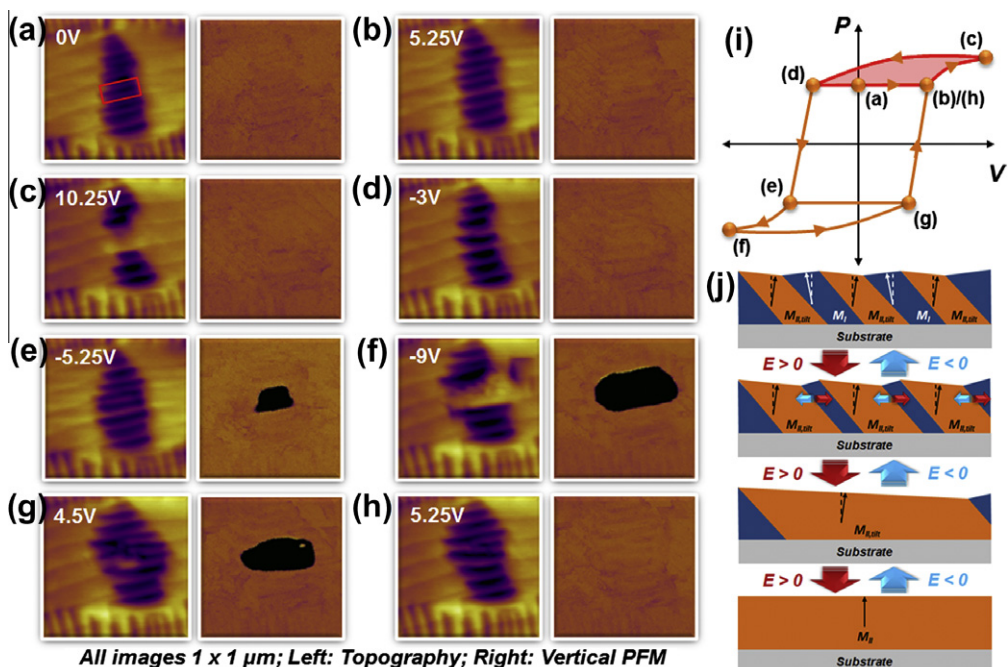


Fig. 9. AFM image (left) and vertical PFM image (right) of 100 nm  $\text{BiFeO}_3/\text{La}_{0.5}\text{Sr}_{0.5}\text{CoO}_3/\text{LaAlO}_3$  (001) in the (a) as-grown state and after being poled in the box at (b) 5.25 V, (c) 10.25 V, (d) -3 V, (e) -5.25 V, (f) -9 V, (g) 4.5 V, and (h) 5.25 V (all images are 1 × 1 μm). (i) A schematic hysteresis loop with letters corresponding to the images in (a)–(h) shows the multiple pathways to enhanced electromechanical response. (j) Illustration of the proposed mechanism for the large electromechanical response without the need for ferroelectric switching (adapted from Ref. [104]).

Raman measurements [106]. Finally there are reports of a concomitant structural and ferroelectric transformation at  $\sim 85$  °C. Based on the study of phonon excitations, as investigated by using Raman scattering as a function of temperature, the low-energy phonon modes related to the  $\text{FeO}_6$  octahedron tilting show anomalous behaviors upon cooling through this temperature – including an increase of intensity by one order of magnitude and the appearance of a dozen new modes [107]. Other recent reports have investigated the emergence of an enhanced spontaneous magnetization in the so-called mixed phase structures [108] and that the magnetic Néel temperature of the strained  $\text{BiFeO}_3$  is suppressed to around room temperature and that the ferroelectric state undergoes a first-order transition to another ferroelectric state simultaneously with the magnetic transition [109]. This has strong implications for room temperature magnetoelectric applications. Finally, other reports have investigated the driving force for the formation of these so-called mixed-phase structures and have revealed that the complex mixed-phase structure likely occurs as the consequence of a strain-induced spinodal instability [110]. Truly this is an exciting and fast-moving field of study today. Such electric-field- and temperature-induced changes of the phase admixture is also reminiscent of the CMR manganites or the relaxor ferroelectrics and is accompanied by large piezoelectric strains, but there appears to be much more to these mixed-phase structures that are a worthy field of further study.

#### 4. Engineering new functionalities with multiferroics

One of the major questions in the study of multiferroics today is how and when will multiferroics make their way

into a room-temperature device and what will these devices look like? In early 2005, a number of so-called magnetoelectronic devices based on magnetoelectric materials were proposed [111]. The idea was a simple one, namely to use the net magnetic moment created by an electric field in a magnetoelectric thin film to change the magnetization of a neighboring ferromagnetic layer through exchange coupling. The authors went on to propose a number of electrically tunable giant magnetoresistance (GMR) spin valves (Fig. 10a) and tunnel magnetoresistance (TMR) (Fig. 10b) elements that could be made possible if such structures could be achieved. One additional field that could be greatly affected by this research is the burgeoning field of spintronics. Spin-based electronics, or spintronics, has already found successful application in magnetic read-heads and sensors that take advantage of GMR and TMR effects [112–114]. The future of spintronics is partially focused on evolving beyond passive magnetoelectronic components, like those used today, to devices which combine memory and logic functions in one [115]. There has been growing interest in studying a direct method for magnetization reversal involving spin transfer from a spin-polarized current injected into the device. This effect has been theoretically predicted by Slonczewski [116,117] and Berger [118], and has been experimentally confirmed by several groups [119–122].

##### 4.1. Electric field vs. current control of magnetism

From these initial experiments and theoretical treatments, it was found that significant current densities (larger than  $10^7 \text{ A cm}^{-2}$ ) were required for switching the orientation of a magnetic nanowire [120]. One option is to further

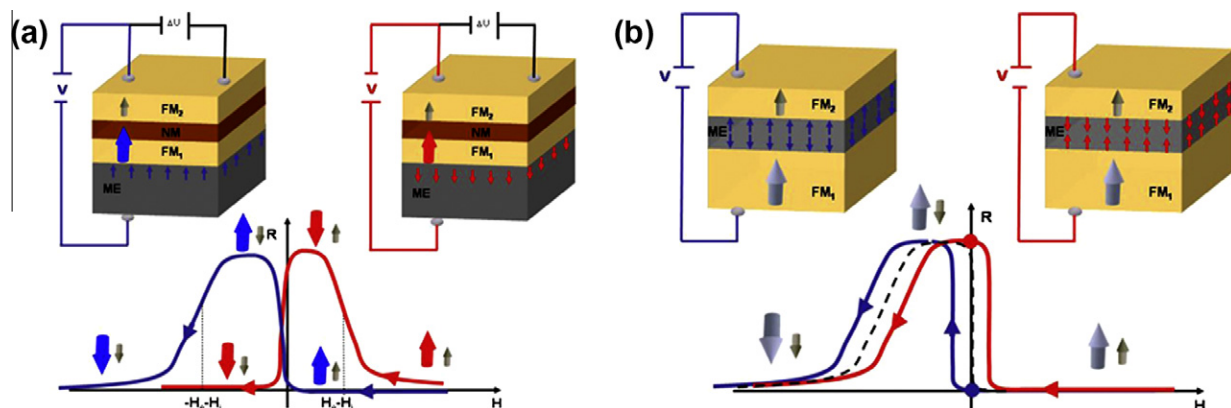


Fig. 10. Multiferroic-based magnetoelectronics. (a) Schematic of the magnetoresistance curve of a GMR device involving a magnetoelectric, multiferroic film as a pinning layer. Half-hysteresis curves are shown, after saturation at positive field values. The change of polarity of the magnetoelectric, multiferroic layer upon application of an electric field changes the direction of the net magnetization of the pinning field. The pinned layer (FM1) switches first at large positive field (red), or second at large negative field (blue). The low field magnetic configuration is therefore either antiparallel (red) or parallel (blue), controlled by the magnetoelectric, multiferroic film. (b) Schematic of the magnetoresistance curve of a TMR device involving a magnetoelectric, multiferroic film as a tunnel barrier. Half-hysteresis curves are shown, after saturation at positive field values. The arrows denote the magnetization directions, with the bottom layer FM1 being harder (or pinned) than the top one FM2. The dashed curve is the expected TMR behavior. The change of voltage polarity changes the direction of the net magnetization of the magnetoelectric, multiferroic layer, adding an exchange bias magnetic field to the resistance curve. The two colors indicate shifting of half-hysteresis curves towards positive or negative fields, depending on the polarity of the applied voltage. At zero magnetic field, the change of voltage polarity changes the resistance value of the device (dashed) (adapted from Ref. [111]). (For interpretation of the references to color in this figure legend, the reader is referred to the web version of this article.)

scale down materials so that spin-transfer becomes a more attractive alternative to stray magnetic field techniques. In the end, integration of such effects into actual devices has been limited because there are a number of technical difficulties involved in reliably making such small structures, applying such large currents – while avoiding heating of the samples, and based on the fact that the intrinsic sample resistance (on the order of a few ohms) further limits the practical use for GMR devices. Similar issues are found in TMR devices, which are hindered by fact that a large current density must pass through a very thin insulator and the few reports on TMR systems to date have been inconclusive [123,124].

#### 4.2. Electric field control of ferromagnetism

The overall motivating question for this section is a simple one: can we deterministically control ferromagnetism at room temperature with an electric field? One possible solution to this question is to utilize heterostructures of existing multiferroic materials, such as BiFeO<sub>3</sub>, to create new pathways to functionalities not presented in nature. Such a concept is illustrated in Fig. 11. The idea is to take advantage of two different types of coupling in materials – intrinsic magnetoelectric coupling like that in multiferroic materials such as BiFeO<sub>3</sub>, which will allow for electrical control of antiferromagnetism, and the extrinsic exchange coupling between ferromagnetic and antiferromagnetic materials – to create new functionalities in materials (Fig. 11a). By utilizing these different types of coupling we can then effectively couple ferroelectric and ferromagnetic order at room temperature and create an alternative pathway to electrical control of ferromagnetism (Fig. 11b). But what exactly are the opportunities for using multiferroics to gain electrical control over interactions like exchange bias anisotropy? Until recently the materials and the understanding of the appropriate materials did not exist to make this a plausible undertaking. Let us investigate, in detail, the work done in this field of study.

#### 4.3. Exchange bias with multiferroic antiferromagnets

In the time since the proposal of these magnetoelectronics, studies have been done on a number of multiferroic

materials. Among the earliest work was a study of heterostructures of the soft ferromagnet permalloy on YMnO<sub>3</sub> [125]. This report found that, indeed, the multiferroic layer could be used as an antiferromagnetic pinning layer that gives rise to exchange bias and enhanced coercivity, but suggested that YMnO<sub>3</sub> would likely be an inappropriate choice for continued study as these values varied greatly with crystal orientation and rendered actual device generation unlikely. Soon after this initial result, Marti et al. [126] reported the observation of exchange bias in all-oxide heterostructure of the ferromagnet SrRuO<sub>3</sub> and the antiferromagnetic, multiferroic YMnO<sub>3</sub>. In both of these studies, the exchange bias existed only at very low temperatures due to the low magnetic ordering temperature of the YMnO<sub>3</sub>. Around the same time, the first studies using BiFeO<sub>3</sub> as the multiferroic, antiferromagnetic layer were appearing with hopes that these intriguing properties could be extended to high temperatures. Dho et al. [127] showed the existence of exchange bias in spin-valve structures based on permalloy and BiFeO<sub>3</sub> at room temperature and Béa et al. [128] extended this idea to demonstrate how BiFeO<sub>3</sub> films could be used in first-generation spintronics devices. This work included the use of ultrathin BiFeO<sub>3</sub> tunnel barriers in magnetic tunnel junctions with La<sub>0.7</sub>Sr<sub>0.3</sub>MnO<sub>3</sub> and Co electrodes where positive TMR up to ~30% was observed at 3 K and also demonstrated that room temperature exchange bias could be generated using CoFeB/BiFeO<sub>3</sub> heterostructures. Finally, Martin et al. [129] reported the growth and characterization of exchange bias and spin valve heterostructures based on Co<sub>0.9</sub>Fe<sub>0.1</sub>/BiFeO<sub>3</sub> heterostructures on Si substrates. In this work large negative exchange bias values (typically 150–200 Oe in magnitude) were observed along with the absence of a training effect – or a systematic decrease in the magnitude of the exchange bias with repeated magnetic cycling (confirming the results of Bea et al. [128]) – even with over 14,000 magnetization reversal cycles. This work also demonstrated room temperature magnetoresistance of ~2.25% for spin valve structures of 2.5 nm Co<sub>0.9</sub>Fe<sub>0.1</sub>/2 nm Cu/5 nm Co<sub>0.9</sub>Fe<sub>0.1</sub>/100 nm BiFeO<sub>3</sub> (Fig. 12). What these initial studies established was that exchange bias with antiferromagnetic multiferroics was possible in a static manner, but these studies had not yet demonstrated dynamic control of exchange coupling in these systems.

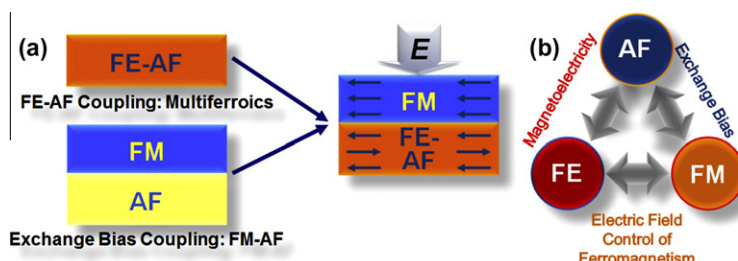


Fig. 11. Schematics illustrating the design algorithm for gaining electrical control of ferromagnetism. (a) By combining multiferroics together with traditional ferromagnets, we can create heterostructures that might have new functionalities. (b) These structures rely on two types of coupling – magnetoelectric and exchange bias – to gain electrical control of ferromagnetism (adapted from Ref. [47]).

A first attempt at this concept was done by Borisov et al. [130], who reported that they could affect changes on the exchange bias field in  $\text{Cr}_2\text{O}_3$  (111)/(Co/Pt)<sub>3</sub> heterostructures by using the magnetoelectric nature of the substrate ( $\text{Cr}_2\text{O}_3$ ) and a series of different cooling treatments with applied electric and magnetic fields. A unique aspect of this work was the ability to change the sign of the exchange bias with different field cooling treatments. Dynamic switching of the exchange bias field with an applied electric field, however, remained elusive until a report by Laukhin et al. [131] focusing on  $\text{YMnO}_3$  at 2 K. Utilizing heterostructures of permalloy and (0001)  $\text{YMnO}_3$  films, the authors demonstrated that after cooling samples from 300 to 2 K in an applied field of 3 kOe and at various applied electric field biases, significant changes in the magnitude of magnetization was observed (Fig. 13a). Subsequent cycling of the voltage at low temperatures resulted in reversal of the magnetization direction in the heterostructure (Fig. 13b).

In the last few years, significant advancement in the understanding of the interactions present in such heterostructures has occurred. Initial reports noted an inverse relationship between domain size in  $\text{BiFeO}_3$  film and the exchange bias measured in CoFeB/ $\text{BiFeO}_3$  heterostructures [132]. This initial report offered little detail on how the domain structures were controlled and the nature of the domain walls present in the films. A study that soon followed found a correlation not only to the density of domain walls, but also to the density of certain types of domain walls [50]. What was observed was the presence of two distinctly different types of magnetic properties for  $\text{Co}_{0.9}\text{Fe}_{0.1}/\text{BiFeO}_3$  heterostructures (Fig. 14a and b). Through careful control of the growth process – specifically controlling the growth rate of the  $\text{BiFeO}_3$  films – the authors were able to create two starkly different types of domains structures: so-called stripe-like (Fig. 14c) and mosaic-like (Fig. 14d) domain structures. These different

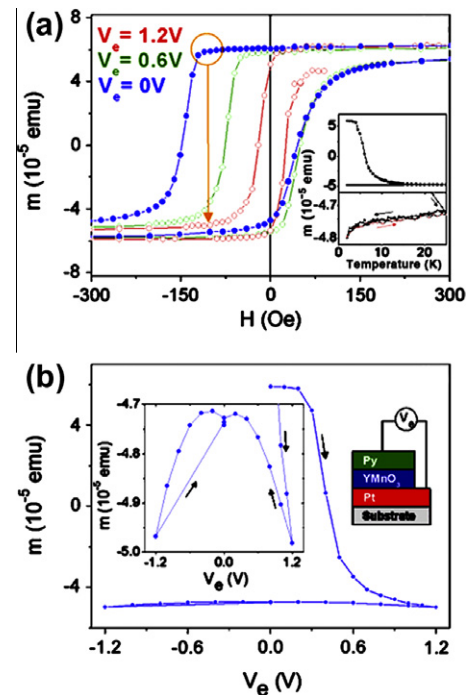


Fig. 13. Low temperature electric field control of ferromagnetism. (a) Magnetization loops for permalloy/YMnO<sub>3</sub>/Pt, measured at 2 K, after cooling the sample from 300 K in a 3 kOe field, under various biasing-voltage ( $V_e$ ) values. The circle and arrow illustrate schematically the expected change of magnetization when biasing the sample by an electric field. The inset shows the temperature dependence of the magnetization at  $H = 100$  Oe and  $V_e = 0$  when heating the sample from 2 K to 25 K (top panel) and subsequent cooling–heating–cooling cycles between 25 K to 2 K (bottom panel). (b) Dependence of the magnetization on  $V_e$  measured at 2 K in  $H = 100$  Oe field after cooling the sample from 300 K in 3 kOe field. The inset shows (left) a zoom of the −1.2 to 1.2 V portions of the bias excursion and (right) a sketch of the sample structure and electric biasing (adapted from Ref. [131]).

structures were found to possess vastly different fractions of the different domain walls that can exist in  $\text{BiFeO}_3$  (Fig. 14e and f). It was observed that not only was there

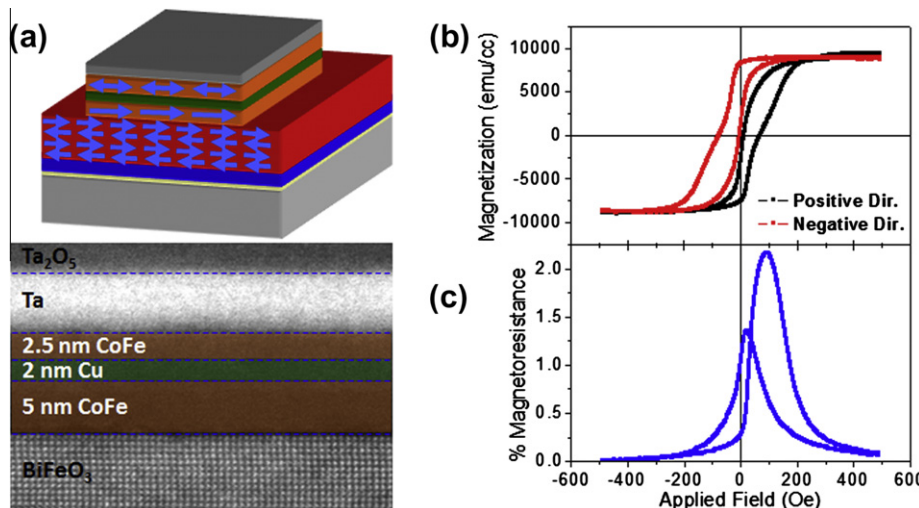


Fig. 12. Spin valve structures based on  $\text{Co}_{0.9}\text{Fe}_{0.1}/\text{Cu}/\text{Co}_{0.9}\text{Fe}_{0.1}/\text{BiFeO}_3$  heterostructures. (a) Schematic illustration and scanning transmission electron microscopy image of the actual device. (b) Magnetic hysteresis loops of spin valve structures. (c) Current-in-plane magnetoresistance measurements (adapted from Ref. [129]).

an inverse relationship between domain size and the magnitude of the exchange bias measured (Fig. 14g), but that it was directly related to the density and total length of 109° domain walls present in the sample (Fig. 14h). In addition to identifying the importance of 109° domain walls in creating exchange bias (and in turn suggesting the relationship with enhanced magnetism in BiFeO<sub>3</sub> thin films), this report outlined the idea that two distinctly different types of exchange interactions are occurring in these exchange bias heterostructures. The first interaction was called an exchange bias interaction and takes place between pinned, uncompensated spin occurring at 109° domain walls in BiFeO<sub>3</sub> and spins in the Co<sub>0.9</sub>Fe<sub>0.1</sub> layer. This interaction results in a shift of the magnetic hysteresis loop for the ferromagnetic layer. The second interaction has been called an exchange enhancement interaction and it arises from an interaction of the spins in the ferromagnet and the fully compensated (001) surface of the G-type anti-ferromagnetic surface of BiFeO<sub>3</sub>. This interaction results in an enhancement of the coercive field of the ferromagnetic layer.

#### 4.4. Room temperature electric field control of ferromagnetic domain structures

Utilizing these findings, researchers have moved to create the first room temperature devices designed to enable control of ferromagnetism with an electric field. Initial results point to the ability to utilize the above exchange enhancement interaction to deterministically change the direction of ferromagnetic domains by 90° upon applica-

tion an applied electric field (Fig. 15) [133]. By creating very high quality Co<sub>0.9</sub>Fe<sub>0.1</sub>/BiFeO<sub>3</sub>/SrRuO<sub>3</sub>/SrTiO<sub>3</sub> (001) heterostructures, the authors were able to demonstrate the first example of a room temperature device structure that utilizes a multiferroic material to access new functionalities in materials. This work also outlined the complexity of such an undertaking. It has become apparent that in order to achieve significant advances with such systems one will need to understand and be able to control (at least at some level) the coupling between the two (in this case dissimilar) materials which requires that one have a perfunctory understanding of the various energies scales at play (including shape anisotropy effects, how processing effects the interfacial coupling strength, magnetostriction effects, and more). This initial work also demonstrated the importance of length scales in this work as the observed ferromagnetic domain structures were typically much more complex than the underlying ferroelectric domain structures, suggesting that diminished feature sizes could give rise to single magnetic domain configurations and therefore a more robust and simple device. In this spirit, current work is focused on making the coupling in such heterostructures more robust in hopes of extending this coupling to high temperatures and producing more deterministic control of electric field switching.

More recently, attention has turned back to one of the earliest studied magnetoelectric materials, Cr<sub>2</sub>O<sub>3</sub>, and a careful study has given rise to exciting work in electric field control of ferromagnetism. Using a combination of modern thin film growth techniques, magnetometry, spin-polarized photoemission spectroscopy, symmetry arguments,

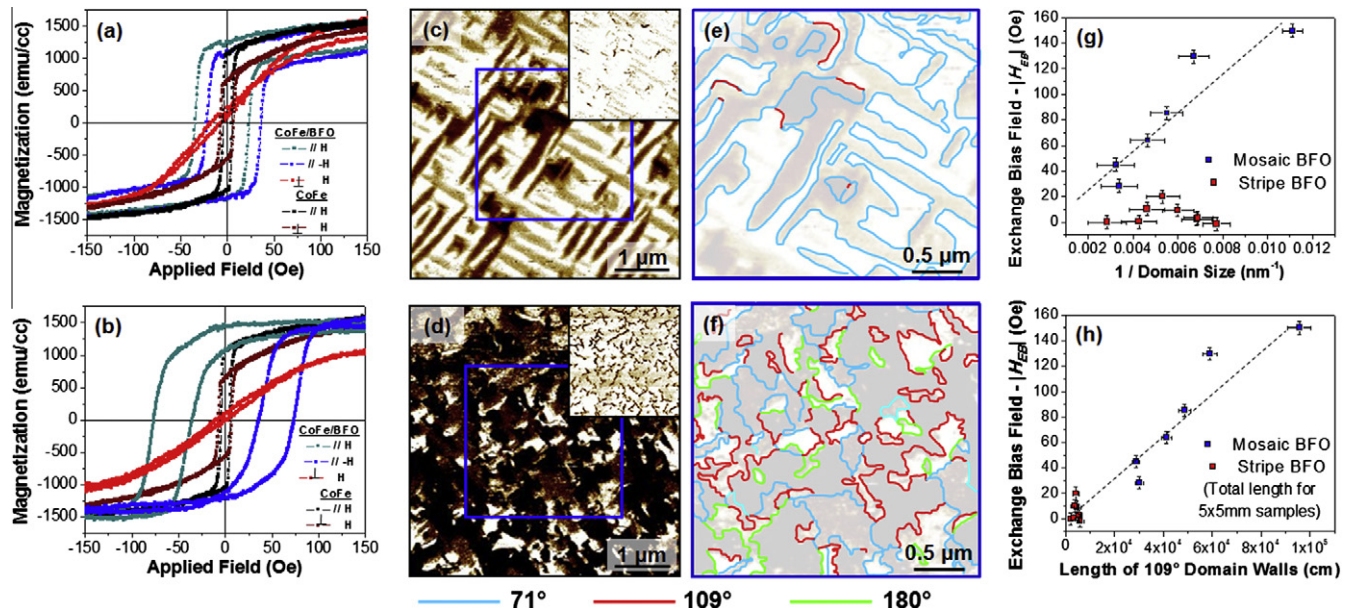


Fig. 14. Domain control of exchange bias. Room temperature magnetic properties for heterostructures exhibiting (a) exchange enhancement and (b) exchange bias properties. In-plane and out-of-plane (inset) PFM contrast for typical BiFeO<sub>3</sub> films that exhibit (c) exchange enhancement and (d) exchange bias, respectively. Detailed domain wall analysis for (e) stripe-like and (f) mosaic-like BiFeO<sub>3</sub> films. (g) Dependence of exchange bias field on domain size for Co<sub>0.9</sub>Fe<sub>0.1</sub>/BiFeO<sub>3</sub> heterostructures grown on mosaic-like (blue) and stripe-like (red) BiFeO<sub>3</sub> films. (h) Exchange bias field of the same samples here graphed as a function of the total length of 109° domain walls/sample surface area in 5 × 5 mm samples (adapted from Ref. [50]). (For interpretation of the references to color in this figure legend, the reader is referred to the web version of this article.)

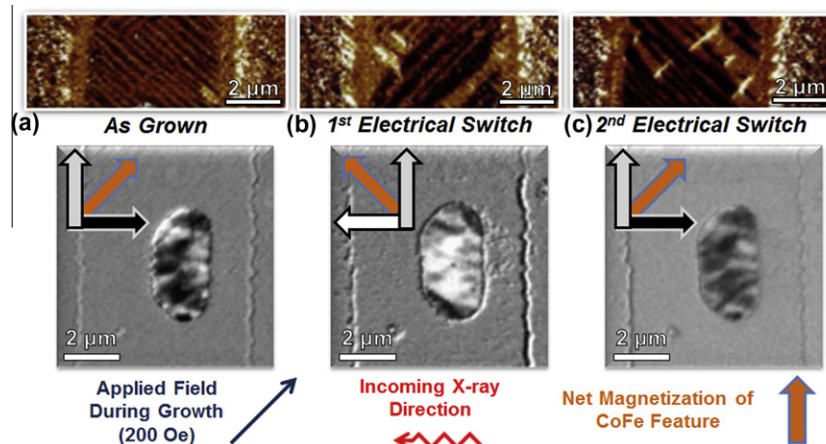


Fig. 15. Electric field control of ferromagnetic domain structures at room temperature. In-plane piezoresponse force microscopy images of ferroelectric domain structure (top) and corresponding photoemission electron microscopy image of ferromagnetic domain structure (bottom) of  $\text{Co}_{0.9}\text{Fe}_{0.1}$  features on  $\text{BiFeO}_3$  as a function of applied electric field in the (a) as-grown state, (b) after application of an electric field, and (c) following application of the opposite electric field. This represents the first demonstration of reversible electric field control of ferromagnetic domain structures at room temperature (adapted from Ref. [133]).

and first-principles, He et al. [134] studied Pd/Co multilayers deposited on (0001) surface of the antiferromagnet  $\text{Cr}_2\text{O}_3$  and demonstrated reversible, room temperature isothermal switching of the exchange bias field from positive to negative values by reversing the electric field under a constant magnetic field. The study revealed that the (0001) surface of  $\text{Cr}_2\text{O}_3$  can be controlled to exhibit a single spin type (Fig. 16a) that gives rise to a strong exchange bias. Magnetic hysteresis loops as a function of various magnetoelectric annealing processes at non-zero electric and magnetic fields reveal the development of exchange bias (Fig. 16b and c), and eventual application of alternating electric fields ( $+2.6 \text{ kV mm}^{-1}$  and  $-2 \text{ kV mm}^{-1}$ ) at a constant magnetic field ( $-154 \text{ mT}$ ) resulted in electric field control of the sign of exchange bias (Fig. 16d).

#### 4.5. Electronic reconstruction and coupling at oxide interfaces

In contrast to the metallic ferromagnet–multiferroic heterostructure described above, one can envision a much broader range of interactions at all-oxide interfaces. The  $\text{La}_{0.7}\text{Sr}_{0.3}\text{MnO}_3$ – $\text{BiFeO}_3$  epitaxial heterostructure presents a good model system to explore such interactions. While exchange coupling at such interfaces typically focuses on the spin degrees of freedom and how they interact at the interface, in oxide systems, especially those with transition metal ions, the orbital and lattice degrees of freedom can be equally active. Recent studies focusing on 20–75 nm  $\text{BiFeO}_3$ /5 nm  $\text{La}_{0.7}\text{Sr}_{0.3}\text{MnO}_3/\text{SrTiO}_3$  (001) heterostructures suggest that by changing the coupling from being direct in nature to indirect across an interface possessing a continuous chemical structure (i.e. Mn–O–Fe bonds that extend across the interface), complex interactions can occur (Fig. 17a) [135]. Through the use of detailed magnetometry, and synchrotron-based X-ray magnetic dichroism studies, the authors reported the formation of a novel ferromagnetic

state in the antiferromagnet  $\text{BiFeO}_3$  at the interface. Using X-ray magnetic circular dichroism at Mn and Fe  $L_{2,3}$  edges (Fig. 17b and c), it was observed that the development of this ferromagnetic spin structure was strongly associated with the onset of a significant exchange bias. The results demonstrate that the magnetic state is directly related to an electronic orbital reconstruction at the interface, which is supported by linearly polarized X-ray absorption measurement at the oxygen K edge. In the end, it is such structures, however, that might represent the ultimate manifestation of new functionality if one can engineer and control these different degrees of freedom to some effect.

#### 4.6. Multiferroic and magnetoelectric devices

Applications of coupled behavior can be broadly classified into the following three groups:

- (i) High-frequency applications – the coupling between the spin and charge lattice (ferroelectromagnons), which typically occurs around 500–1000 GHz, is then modulated with an electric or magnetic field, akin to FMR devices. A related manifestation is a ferromagnet–multiferroic heterostructure in which resonance in the ferromagnetic layer is controlled by an electric field applied to the multiferroic.
- (ii) A second class of applications relates to the control of spin transport with electric fields, in either a tunnel junction or spin valve geometry.
- (iii) A third manifestation would be the use of such multiferroics in information storage elements, similar to a nonvolatile ferroelectric memory (FRAM), but one in which both the magnetic and ferroelectric state are used, either independently or in unison.

The potential applications of multiferroics and magnetoelectrics were reviewed by Scott [136]. It is important

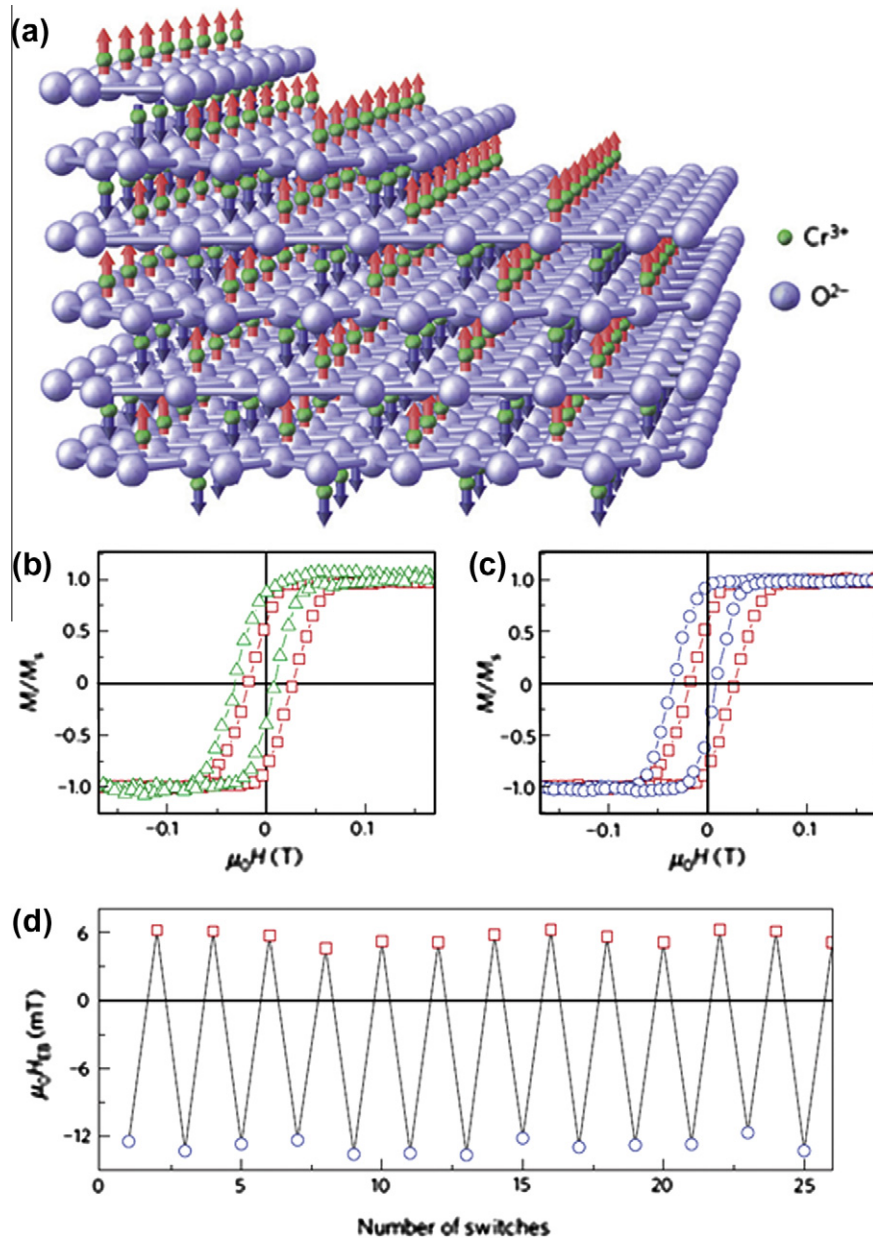


Fig. 16. Electric field control of magnetism with Cr<sub>2</sub>O<sub>3</sub>. (a) The spin structure of a Cr<sub>2</sub>O<sub>3</sub> single crystal with a terraced (0001) surface is shown for one of its two antiferromagnetic single-domain states. Up (red) and down (dark blue) spins of the Cr<sup>3+</sup> ions (green spheres) point along the *c* axis. (b) Exchange-biased hysteresis loops of Cr<sub>2</sub>O<sub>3</sub> (0001)/Pd 0.5 nm/(Co 0.6 nm/Pd 1.0 nm)<sub>3</sub> at *T* = 303 K after initial magnetoelectric annealing in *E* = 0.1 kV mm<sup>-1</sup> and *H* = 77.8 mT. Hysteresis loops are measured by polar Kerr magnetometry at *E* = 0. The red squares show the virgin curve with a positive exchange-bias field of +6 mT. Isothermal-field exposure in *E* = -2.6 kV mm<sup>-1</sup> and *H* = 154 mT gives rise to a loop with a negative exchange-bias field of -13 mT (green triangles). (c) The red squares show the same virgin reference loop. The blue circles show the hysteresis loop after isothermal-field exposure in *E* = 2.6 kV mm<sup>-1</sup> and *H* = -154 mT, giving rise to the same negative exchange bias of -13 mT. (d) Exchange bias field vs. number of repeated isothermal switching through exposure to *E* = 2.6 kV mm<sup>-1</sup> (blue circles) and -2 kV mm<sup>-1</sup> (red squares) at constant *H* = -154 mT, respectively (adapted from Ref. [134]). (For interpretation of the references to color in this figure legend, the reader is referred to the web version of this article.)

to note that although ferroelectric random access memories (FeRAMs) have achieved fast access speeds (5 ns) and high densities (64 Mb) in a number of different materials, they remain limited by the need for a destructive read and reset operation. The appeal of multiferroics is that they offer the possibility of combining the best qualities of FeRAMs and MRAMs: fast low-power electrical write operation, and

non-destructive magnetic read operation. At the 256 Mbit level, such memory devices [137] would be a “disruptive technology” and could eliminate competition such as EEPROMs (electrically erasable programmable read-only memories) for applications including megapixel photomemories for digital cameras or audio memories in devices such as mp3 players. It is fair to state, however, that work

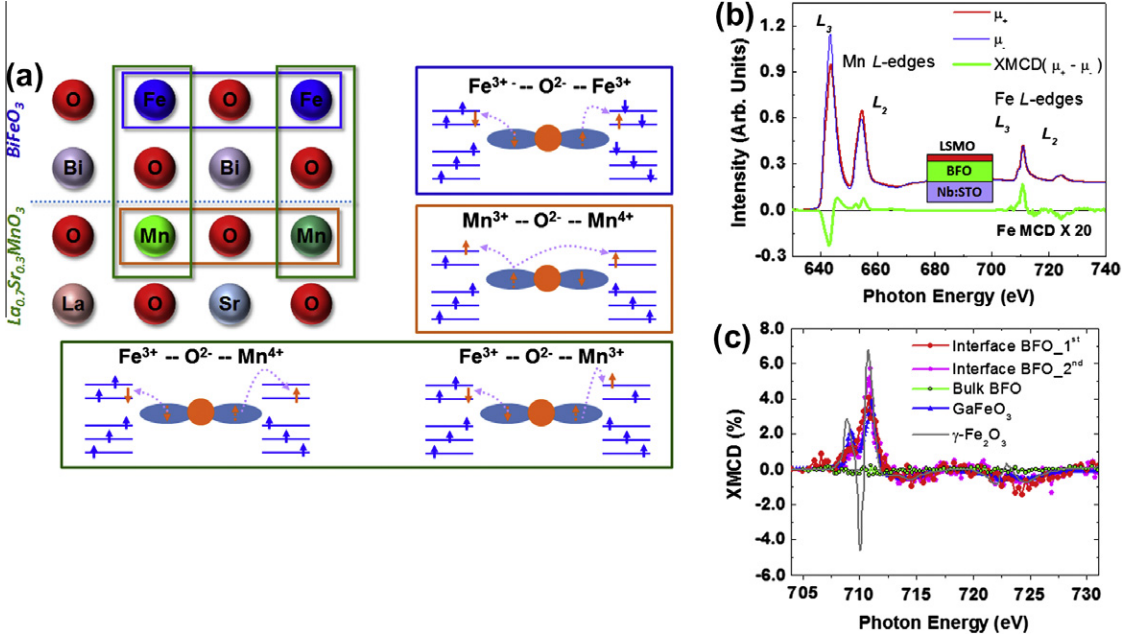


Fig. 17. Magnetic coupling across all-oxide interfaces. (a) Schematic illustrating the complexity of all-oxide interfaces in multiferroic-based heterostructures. In all-oxide heterostructures there is competition between different types of indirect coupling: antiferromagnetic superexchange in BiFeO<sub>3</sub> (blue box), ferromagnetic double exchange in La<sub>0.7</sub>Sr<sub>0.3</sub>MnO<sub>3</sub> (orange box), and cross-interface coupling between Fe<sup>3+</sup>-Mn<sup>3+</sup> and Fe<sup>3+</sup>-Mn<sup>4+</sup> (green box). (b) X-ray absorption spectroscopy and magnetic circular dichroism (XMCD) spectra of Mn and Fe L<sub>2,3</sub> edges taken at 10 K. The XMCD signal of Fe is multiplied by a factor of 20. (c) Comparison of the interface Fe XMCD with bulk BiFeO<sub>3</sub>, GaFeO<sub>3</sub> and γ-Fe<sub>2</sub>O<sub>3</sub>. The spectra of GaFeO<sub>3</sub> and γ-Fe<sub>2</sub>O<sub>3</sub> are normalized to the same scale as that of interface BiFeO<sub>3</sub> state (adapted from Ref. [135]). (For interpretation of the references to color in this figure legend, the reader is referred to the web version of this article.)

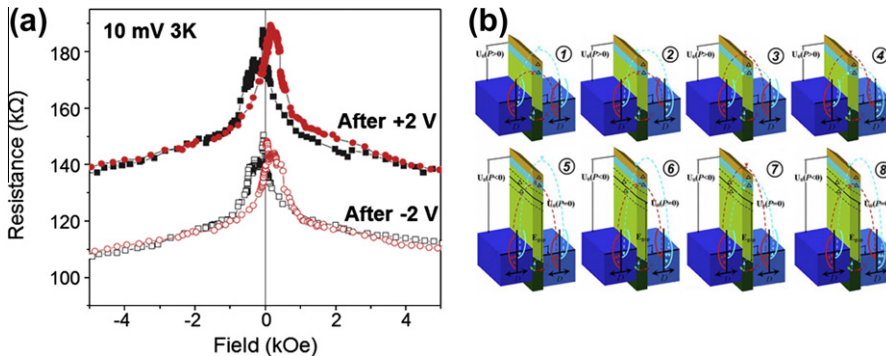


Fig. 18. Multiferroic-based devices. (a) Tunnel magnetoresistance curves at 4 K at  $V_{dc} = 10$  mV in an La<sub>2/3</sub>Sr<sub>1/3</sub>MnO<sub>3</sub>/La<sub>0.1</sub>Bi<sub>0.9</sub>MnO<sub>3</sub> (2 nm)/Au junction, after applying a voltage of +2 V (filled symbols) and -2 V (open symbols). The combination of the electroresistance effect and the tunnel magnetoresistance produces a four-resistance-state system (adapted from Ref. [139]). (b) The sketch of the potential profiles for each of the eight configurations of a multiferroic-based tunnel junction. Here, the red and light blue arrows denote majority- and minority-spin carriers, and  $D$  displays the electronic density of states (adapted from Ref. [140]). (For interpretation of the references to color in this figure legend, the reader is referred to the web version of this article.)

on possible applications is still in its infancy and the field would benefit significantly with strong device-related research.

Over the last few years, a number of new devices based on multiferroic materials and heterostructures have been demonstrated and proposed. In early 2007, Ju et al. [138] presented a theoretical investigation of an electrically controllable spin filter based on a multiferroic tunnel junction that could be switched between multiple resistance states. Soon after this, Gajek et al. [139] demonstrated the produc-

tion of four logic states based on ultrathin multiferroic films used as barriers in spin-filter-type tunnel junctions. The junctions were made of La<sub>0.1</sub>Bi<sub>0.9</sub>MnO<sub>3</sub>, which was proven to be both ferroelectric and magnetic down to film thickness of only 2 nm and the devices exploited the magnetic and ferroelectric degrees of freedom of that layer. The ferromagnetism permitted read operations reminiscent of MRAM and the electrical switching evoked FeRAM write operations without the need for destructive ferroelectric readout. The results (Fig. 18a) suggest that it is possible

to encode quaternary information by both ferromagnetic and ferroelectric order parameters, and to read it non-destructively by a resistance measurement. This work represented the starting point for future studies on the interplay between ferroelectricity and spin-dependent tunneling using multiferroic barrier layers and in a wider perspective, suggested a new pathway toward novel reconfigurable logic spintronic architectures.

Yang et al. [140] proposed that eight different logic states could be achieved by combining spin-filter effects and the screening of polarization charges between two electrodes through a multiferroic tunnel barrier (Fig. 18b). In this work, the conductance ratio was found to be dependent on the magnitude of the ferroelectric polarization, exchange splitting, barrier width, and bias voltage. In 2009, Jia and Berakdar [141] proposed a modified spin-field-effect transistor fabricated in a two-dimensional electron gas (2DEG) formed at the surface of multiferroic oxides with a transverse helical magnetic order. The local magnetic moments in the oxide are said to induce a resonant momentum-dependent effective spin-orbit interaction acting on the 2DEG and thus the carrier spin precession is dependent on the magnetic spin helicity that can be electrically controlled in the multiferroic. Such a device could, in turn, be used as a nanometer-scale, decoherence-suppressed spin field-effect transistor and as a nanometer flash-memory device.

## 5. Future directions and conclusions

We hope that this review has captured some of the exciting new developments in the field of complex oxides, multiferroics and magnetoelectrics, especially from a thin film perspective. New developments are occurring at a rapid pace, throwing further light onto the complexities inherent to these materials. The dramatic progress in thin film heterostructure and nanostructure growth has been a key enabler fueling these discoveries. Since the advent of the superconducting cuprates, complex oxides have emerged as wonderful tools to probe the role of complexity induced by the interactions between the spin, charge, orbital, and lattice degrees of freedom that are pervasive in transition metal oxides. Soon after the cuprates, work on ferroelectric oxides emerged, followed by the colossal magnetoresistance effect in the doped manganites. Transitioning fundamental materials discoveries into real products involves many steps, including pathways to design and create device structures that can then be inserted into systems architectures and the understanding of how these new technologies impact existing markets. A continued limitation of investment into manufacturing may remain a concern for the oxide field for years to come.

In turn, one of the biggest challenges facing the field of multiferroics today is the need for room temperature function. Thus, it is essential that the field works to include both thin film heterostructure and bulk synthesis methods and broadens the search for new candidate multiferroics.

The interplay between ab initio, density functional theoretical approaches and controlled synthetic approaches (be it single crystal growth or MBE-like heteroepitaxial thin film growth) is critical. Thin film heterostructures further provide an additional degree of freedom through the mismatch strain; here again, the intimate interplay between theoretical predictions [142] and film growth is imperative. If deterministic control and manipulation of ferromagnetism are desired, then interactions across heterointerfaces will become important as we attempt to design systems capable of these functionalities. Domains, domain walls, and defects will undoubtedly play a critical role in unraveling the coupling phenomena. Further, in such heterostructure-based coupling, differences between interactions with classical itinerant ferromagnets and double exchange ferromagnets (such as the manganite) need to be explored in depth as well. In thin films, heteroepitaxial constraints (such as strain, clamping, and possibly surface termination) are important variables. This is truly a challenge for interdisciplinary condensed matter research.

At a more fundamental science level, complex oxides provide a versatile class of materials for the exploration of coupling and interplay amongst charge, spin, orbital, and lattice degrees of freedom. These interactions lead to novel (and exotic) ground states for the system that can be manipulated by external perturbations. The ability to engineer artificial heterostructures down to the unit cell level through MBE and related techniques provides unprecedented access to quantum phenomena in oxides. At the crystal chemistry level, the interplay between cationic sizes and oxygen coordination chemistry leads to tilts and rotations of the oxygen octahedra. Control and manipulation of these degrees of freedom, especially at heterointerfaces where symmetry breaking is easily achieved, has captured the interest of researchers in the field and is likely to be an active area of research. The orbital degree of freedom, however, is still a relatively less explored aspect. An ideal manifestation would be room temperature electric field control of the orbital order in perovskites such as the manganites. Another area that presents both scientific challenges and opportunities relates to the properties of domain walls, especially conduction at domain walls in otherwise insulating ferroelectrics. A critical question is this: can we possibly create an insulator–metal transition at the wall, i.e. can the walls exhibit metallic conduction? If this is possible through careful control of the electronic structure at the wall as well as through external constraints (epitaxy, defect chemistry, etc.), this is likely to be a major breakthrough, since the domain walls in ferroelectrics are truly “nano-objects” (width of the order of a few nm) and they can be manipulated (written, erased and relocated) using electric fields.

In the end, as we look back at the development of complex oxide research we see that a series of exciting discoveries, from high  $T_C$  superconductivity to multiferroism, has propelled the greater field of oxides to the forefront of condensed matter physics. The diverse functionality of

oxide materials means that this breakthrough could drive the field towards many of the major scientific questions that face us today – from energy, to medicine, to communications, and beyond.

## Acknowledgements

L.W.M. acknowledges the support of the Army Research Office under Grant W911NF-10-1-0482 and the Samsung Electronics Co. Ltd under Grant 919 Samsung 2010-06795. R.R. acknowledges the support of the Director, Office of Basic Energy Sciences, Materials Science Division of the US Department of Energy under Contract No. DE-AC02-05CH11231, support from several ARO and ONR MURI contracts, and the Western Institute of Nanoelectronics program, as well as significant intellectual and financial support from scientists and engineers at Intel. R.R. has also benefitted significantly through funding from the National Science Foundation during his tenure at the University of Maryland, College Park. Both authors have benefitted from the numerous collaborations within the program at Berkeley/LBNL, as well as with valued collaborators around the world.

## References

- [1] Rao CNR, Raveau B. Transition metal oxides. New York: Wiley-VCH; 1998.
- [2] Norton D. Mater Sci Eng R 2004;43:139.
- [3] Smyth DM. The defect chemistry of metal oxides. New York: Oxford University Press; 2000.
- [4] Imada M, Fujimori A, Tokura Y. Rev Mod Phys 1998;70:1039.
- [5] Goodenough JB. Prog Solid State Chem 1971;5:145.
- [6] Kilner JA, Brook RJ. Solid State Ionics 1982;6:237.
- [7] Timusk T, Statt B. Rep Prog Phys 1999;62:61.
- [8] Tsuei CC, Kirtley JR. Rev Mod Phys 2000;72:969.
- [9] Lee PA, Nagaosa N, Wen XG. Rev Mod Phys 2006;78:17.
- [10] Dagotto E. Nanoscale phase separation and colossal magnetoresistance. New York: Springer Verlag; 2003.
- [11] Sorensen OT. Nonstoichiometric oxides. New York: Academic Press; 1981.
- [12] Schmid H. Ferroelectrics 1994;162:665.
- [13] Fiebig M. J Phys D 2005;38:R123.
- [14] Eerenstein W, Mathur ND, Scott JF. Nature 2006;442:759.
- [15] Spaldin NA, Cheong SW, Ramesh R. Phys Today 2010;63:38.
- [16] Cheong SW, Mostovoy M. Nature Mater 2007;6:13.
- [17] Royen P, Swars K. Angew Chem 1957;24:779.
- [18] Kubel F, Schmid H. Acta Crystallogr 1990;B46:698.
- [19] Kiselev SV, Ozerov RP, Zhdanov GS. Sov Phys Dokl 1963;7:742.
- [20] Teague JR, Gerson R, James WJ. Solid State Commun 1963;8:1073.
- [21] Michel C, Moreau JM, Achenbach GD, Gerson R, James WJ. Solid State Commun 1969;7:701.
- [22] Moreau JM, Michel C, Gerson R, James WJ. J Phys Chem Solids 1971;32:1315.
- [23] Zavaliche F, Yang SY, Zhao T, Chu YH, Cruz MP, Eom CB, et al. Phase Transit 2006;79:991.
- [24] Fischer P, Polomska M, Sosnowska I, Szymanski M. J Phys C 1980;13:1931.
- [25] Sosnowska I, Peterlin-Neumaier T, Steichele E. J Phys C 1982;15:4835.
- [26] Dzyaloshinskii IE. Sov Phys JETP 1957;5:1259.
- [27] Moriya T. Phys Rev 1960;120:91.
- [28] Wang J, Neaton JB, Zheng H, Nagarajan V, Ogale SB, Liu B, et al. Science 2003;299:1719.
- [29] Lebeugle D, Colson D, Forget A, Viret M, Bonville P, Marucco JF, et al. Phys Rev B 2007;76:024116.
- [30] Neaton JB, Ederer C, Waghmare UV, Spaldin NA, Rabe KM. Phys Rev B 2005;71:014113.
- [31] Ederer C, Spaldin NA. Phys Rev B 2005;71:060401(R).
- [32] Eerenstein W, Morrison FD, Dho J, Blamire MG, Scott JF, Mathur ND. Science 2005;307:1203a.
- [33] Béa H, Bibes M, Fusil S, Bouzehouane K, Jacquet E, Rode K, et al. Phys Rev B 2006;74:020101.
- [34] Wang J, Scholl A, Zheng H, Ogale SB, Viehland D, Schlom DG, et al. Science 2005;307:1203b.
- [35] Gao F, Chen X, Yin K, Dong S, Ren Z, Yuan F, et al. Adv Mater 2007;19:2889.
- [36] Kabelac J, Ghosh S, Dobal PS, Katiyar R. J Vac Sci Technol B 2007;25:1049.
- [37] Ihlefeld JF, Kumar A, Gopalan V, Schlom DG, Chen YB, Pan XQ, et al. Appl Phys Lett 2007;91:071922.
- [38] Palkar VR, John J, Pinto R. Appl Phys Lett 2002;80:1628.
- [39] Lee YH, Lee CC, Liu ZX, Liang CS, Wu JM. Electrochim Solid State Lett 2005;8:F55.
- [40] Das RR, Kim DM, Baek SH, Zavaliche F, Yang SY, Ke X, et al. Appl Phys Lett 2006;88:242904.
- [41] Yang SY, Zavaliche F, Mohaddes-Ardabili L, Vaithyanathan V, Schlom DG, Lee YJ, et al. Appl Phys Lett 2005;87:102903.
- [42] Ueno R, Okaura S, Funakubo H, Saito K. Jpn J Appl Phys 2005;44:L1231.
- [43] Singh SK, Kim YK, Funakubo H, Ishiwara H. Appl Phys Lett 2006;88:062502.
- [44] Wang J, Zheng H, Ma Z, Prasertchoung S, Wuttig M, Droopad R, et al. Appl Phys Lett 2004;85:2574.
- [45] Tian W, Vaithyanathan V, Schlom DG, Zhan Q, Yang SY, Chu YH, et al. Appl Phys Lett 2007;90:172908.
- [46] Chu YH, Zhao T, Cruz MP, Zhan Q, Yang PL, Martin LW, et al. Appl Phys Lett 2007;90:252906.
- [47] Martin LW, Crane SP, Chu YH, Holcomb MB, Gajek M, Huijben M, et al. J Phys Condens Matter 2008;20:434220.
- [48] Sun HP, Tian W, Pan XQ, Haeni JH, Schlom DG. Appl Phys Lett 2004;84:3298.
- [49] Holcomb MB, Martin LW, Scholl A, He Q, Yu P, Yang CH, et al. Phys Rev B 2010;81:134406.
- [50] Martin LW, Chu YH, Holcomb MB, Huijben M, Han SJ, Lee D, et al. Nano Lett 2008;8:2050.
- [51] Přívratská J, Janovec V. Ferroelectrics 1997;204:321.
- [52] Přívratská J, Janovec V. Ferroelectrics 1999;222:23.
- [53] Baryakhtar VG, L'vov VA, Yablonskii DA. Zh Eksp Teor Fiz 1984;87:1863.
- [54] Thomas L, Hayashi M, Jiang X, Moriya R, Rettner C, Parkin S. Science 2007;315:1553.
- [55] Goltsev V, Pisarev RV, Lottermoser T, Fiebig M. Phys Rev Lett 2003;90:177204.
- [56] Mostovoy M. Phys Rev Lett 2006;96:067601.
- [57] Aird A, Salje EKH. J Phys: Condens Matter 1998;10:L377.
- [58] Bartels M, Hagen V, Burianek M, Getzlaff M, Bismayer U, Wiesendanger R. J Phys: Condens Matter 2003;15:1957.
- [59] Zubko P, Catalan G, Buckley A, Welche PRL. Phys Rev Lett 2007;99:167601.
- [60] Daraktchiev M, Catalan G, Scott JF. Ferroelectrics 2008;375:122.
- [61] Catalan G, Scott JF. Adv Mater 2009;21:2463.
- [62] He Q, Yeh CH, Yang JC, Singh-Bhalla G, Liang CW, Chiu PW, et al. Phys Rev Lett 2011, accepted for publication.
- [63] Seidel J, Martin LW, He Q, Zhan Q, Chu YH, Rother A, et al. Nature Mater 2009;8:229.
- [64] Meyer B, Vanderbilt D. Phys Rev B 2002;65:104111.
- [65] Zhao T, Scholl A, Zavaliche F, Lee K, Barry M, Doran A, et al. Nature Mater 2006;5:823.

- [66] Lebeugle D, Colson D, Forget A, Viret M, Bataille AM, Gukasov A. *Phys Rev Lett* 2008;100:227602.
- [67] van den Boomgaard J, Terrell DR, Born RAJ. *J Mater Sci* 1974;9:1705.
- [68] Avellaneda M, Harshe G. *J Intel Mater Syst Str* 1994;5:501.
- [69] Ryu J, Priya S, Carazo AV, Uchino K, Kim H. *J Am Ceram Soc* 2001;84:2905.
- [70] Ryu S, Park JH, Jang HM. *Appl Phys Lett* 2007;91:142910.
- [71] Ryu J, Carazo AV, Uchino K, Kim H. *J Electroceram* 2001;7:17.
- [72] Srinivasan G, Rasmussen ET, Gallegos J, Srinivasan R. *Phys Rev B* 2001;64:214408.
- [73] Srinivasan G, Rasmussen ET, Levin BJ, Hayes R. *Phys Rev B* 2002;65:134402.
- [74] Srinivasan G, Rasmussen ET, Bush AA, Kamentsev KE. *Appl Phys A* 2004;78:721.
- [75] Ryu J, Priya S, Uchino K, Kim HE. *J Electroceram* 2002;8:107.
- [76] Murugavel P, Singh MP, Prellier W, Mercey B, Simon C, Raveau B. *J Appl Phys* 2005;97:103914.
- [77] Stein S, Wuttig M, Viehland D, Quandt E. *J Appl Phys* 2005;97:10Q301.
- [78] Bichurin MI, Petrov VM, Srinivasan G. *Phys Rev B* 2003;68:054402.
- [79] Zheng H, Wang J, Lofland SE, Ma Z, Mohaddes-Ardabili L, Zhao T, et al. *Science* 2004;303:661.
- [80] Zheng H, Zhan Q, Zavaliche F, Sherburne M, Straub F, Cruz MP, et al. *Nanoletter* 2006;7:1401.
- [81] Li J, Levin I, Slutsker J, Provenzano V, Schenck PK, Ramesh R, et al. *Appl Phys Lett* 2005;87:072909.
- [82] Wan JG, Wang XW, Wu YJ, Zeng M, Wang Y, Jiang H, et al. *Appl Phys Lett* 2005;86:122501.
- [83] Ren S, Wuttig M. *Appl Phys Lett* 2007;91:083501.
- [84] Zhan Q, Yu R, Crane SP, Zheng H, Kisielowski C, Ramesh R. *Appl Phys Lett* 2006;89:172902.
- [85] Murakami M, Fujino S, Lim SH, Salamanca-Riba LG, Wuttig M, Takeuchi I, et al. *Appl Phys Lett* 2006;88:112505.
- [86] Ryu H, Murugavel P, Lee JH, Chae SC, Noh TW, Oh YS, et al. *Appl Phys Lett* 2006;89:102907.
- [87] Wan JG, Weng Y, Wu Y, Li Z, Liu JM, Wang G. *Nanotechnology* 2007;18:465708.
- [88] Nan C-W, Bichurin MI, Dong S, Viehland D, Srinivasan G. *J Appl Phys* 2008;103:031101.
- [89] Zavaliche F, Zheng H, Mohaddes-Ardabili L, Yang SY, Zhan Q, Shafer P, et al. *Nano Lett* 2005;5:1793.
- [90] Zavaliche F, Zhao T, Zheng H, Straub F, Cruz MP, Yang PL, et al. *Nano Lett* 2007;7:1586.
- [91] Tsui DC, Stormer HL, Gossard AC. *Phys Rev Lett* 1982;48:1559.
- [92] Ederer C, Spaldin NA. *Phys Rev Lett* 2005;95:257601.
- [93] Ravindran P, Vidya R, Kjekshus A, Fjellvåg H. *Phys Rev B* 2006;74:224412.
- [94] Ricinschi D, Yun KY, Okuyama M. *J Phys: Condens Matter* 2006;18:L97.
- [95] Béa H, Dupé B, Fusil S, Mattana R, Jacquet E, Warot-Fonrose B, et al. *Phys Rev Lett* 2009;102:217603.
- [96] Zeches RJ, Rossell MD, Zhang JX, Hatt AJ, He Q, Yang CH, et al. *Science* 2009;326:977.
- [97] Roytburd AL. *J Appl Phys* 1998;83:228.
- [98] Alpay SP, Roytburd AL. *J Appl Phys* 1998;83:4714.
- [99] Zhang JX, Xiang B, He Q, Seidel J, Zeches RJ, Yu P, et al. *Nature Nanotechnol* 2011;6:98.
- [100] Dupé B, Infante IC, Geneste G, Janolin PE, Bibes M, Barthélémy A, et al. *Phys Rev B* 2010;81:144128.
- [101] Mazumdar D, Shelke V, Iliev M, Jesse S, Kumar A, Kalinin SV, et al. *Nano Lett* 2010;10:2555.
- [102] Christen H, Nam JH, Kim HS, Hatt AJ, Spaldin NA. *Phys Rev B* 2011;83:144107.
- [103] Chen Z, Luo Z, Huang C, Qi Y, Yang P, You L, et al. *Adv Funct Mater* 2011;21:133.
- [104] Damodaran AR, Liang CW, He Q, Peng CY, Chang L, Chu YH, et al. *Adv Mater* 2011;23:3170.
- [105] MacDougall GW, Christen HM, Siemons W, Biegalski MD, Zarestky JL, Liang S, et al. arXiv: 1107.2975v1.
- [106] Kreisel J, Jadhav P, Chaix-Pluchery O, Varela M, Dix N, Sanchez F, et al. *J Phys Condens Matter* 2011;23:342202.
- [107] Choi KY, Do SH, Lemmens P, Wulferding D, Woo CS, Lee JH, et al. *Phys Rev B* 2011;84:132408.
- [108] He Q, Chu YH, Heron JT, Yang SY, Liang WI, Kuo CY, et al. *Nature Commun* 2011;2:225.
- [109] Ko KT, Jung MH, He Q, Lee JH, Woo CS, Chu K, et al. *Nature Commun* 2011;2:567.
- [110] Damodaran AR, Lee S, Kartik J, MacClaren S, Martin LW. *Phys Rev B*, accepted for publication. arXiv:1110.3847v1 [cond-mat.mtrl-sci].
- [111] Binek C, Doudin B. *J Phys: Condens Matter* 2005;17:L39.
- [112] Nogués J, Schuller IK. *J Magn Magn Mater* 1999;192:203.
- [113] Wolf SA, Awschalom DD, Buhrman RA, Daughton JM, von Molnár S, Roukes ML, et al. *Science* 2001;294:1488.
- [114] Shinjo T. *Nanomagnetism and spintronics*. Oxford: Elsevier; 2009.
- [115] Ney A, Pampuch C, Koch R, Ploog KH. *Nature* 2003;425:485.
- [116] Slonczewski J. *J Magn Magn Mater* 1996;159:L1.
- [117] Slonczewski J. *J Magn Magn Mater* 1999;195:261.
- [118] Berger L. *Phys Rev B* 1996;54:9353.
- [119] Tsoi M, Jansen AGM, Chiang WC, Seck M, Tsoi V, Wyder P. *Phys Rev Lett* 1998;80:4281.
- [120] Wegrowe JE, Kelly D, Jaccard Y, Guittienne P, Ansermet JP. *Europhys Lett* 1999;45:626.
- [121] Myers EB, Ralph DC, Katine JA, Louie RN, Buhrman RA. *Science* 1999;285:867.
- [122] Urazhdin S, Birge NO, Pratt Jr WP, Bass J. *Phys Rev Lett* 2003;91:146803.
- [123] Liu Y, Zhang Z, Freitas PP, Martins JL. *Appl Phys Lett* 2003;82:2871.
- [124] Huai Y, Albert F, Nguyen P, Pakala M, Valet T. *Appl Phys Lett* 2004;84:3118.
- [125] Dho J, Blamire MG. *Appl Phys Lett* 2005;87:252504.
- [126] Martí X, Sánchez F, Fontcuberta J, García-Cuenca MV, Ferrater C, Varela M. *J Appl Phys* 2006;99:08P302.
- [127] Dho J, Qi X, Kim H, MacManus-Driscoll JL, Blamire MG. *Adv Mater* 2006;18:1445.
- [128] Béa H, Bibes M, Cherifi S. *Appl Phys Lett* 2006;89:242114.
- [129] Martin LW, Chu YH, Zhan Q, Ramesh R, Han SJ, Wang SX, et al. *Appl Phys Lett* 2007;91:172513.
- [130] Borisov P, Hochstrat A, Chen X, Kleeman W, Binek C. *Phys Rev Lett* 2005;94:117203.
- [131] Laukhin V, Skumryev V, Martí X, Hrabovsky D, Sánchez F, García-Cuenca MV, et al. *Phys Rev Lett* 2006;97:227201.
- [132] Béa H, Bibes M, Ott F, Dupé B, Zhu XH, Petit S, et al. *Phys Rev Lett* 2008;100:017204.
- [133] Chu YH, Martin LW, Holcomb MB, Gajek M, Han SJ, Balke N, et al. *Nature Mater* 2008;7:478.
- [134] He X, Wang Y, Wu N, Caruso AN, Vescovo E, Belashchenko KD, et al. *Nature Mater* 2010;9:579.
- [135] Yu P, Lee JS, Okamoto S, Rossell MD, Huijben M, Yang CH, et al. *Phys Rev Lett* 2010;105:027201.
- [136] Scott JF. *Nature Mater* 2007;6:256.
- [137] Cristensen CM. *The innovator's dilemma*. Boston (MA): Harvard Business School Press; 1997.
- [138] Ju S, Cai TY, Guo GY, Li ZY. *Phys Rev B* 2007;75:064419.
- [139] Gajek M, Bibes M, Fusil S, Bouzehouane K, Fontcuberta J, Barthelemy A, et al. *Nature Mater* 2007;6:296.
- [140] Yang F, Tang MH, Ye Z, Zhou YC, Zheng XJ, Zheng JX, et al. *J Appl Phys* 2007;102:044504.
- [141] Jia C, Berakdar J. *Appl Phys Lett* 2009;95:012105.
- [142] Fennie CJ, Rabe KM. *Phys Rev Lett* 2007;97:267602.